

DOKUZ EYLÜL UNIVERSITY
GRADUATE SCHOOL OF NATURAL AND APPLIED SCIENCES

**ANALYSIS AND CONTROL OF SINGLE-PHASE
GRID CONNECTED MODULAR MULTILEVEL
CONVERTER**



by

Elif BEYHAN ÇERÇİ

September, 2019

İZMİR

ANALYSIS AND CONTROL OF SINGLE-PHASE GRID CONNECTED MODULAR MULTILEVEL CONVERTER

**A Thesis Submitted To The
Graduate School Of Natural And Applied Sciences Of Dokuz Eylül University
In Partial Fulfillment Of The Requirements For The Master Of Science In
Electrical And Electronics Engineering Program**

**by
Elif BEYHAN ÇERÇİ**

**September, 2019
İZMİR**

M.Sc THESIS EXAMINATION RESULT FORM

We have read the thesis entitled “ANALYSIS AND CONTROL OF SINGLE-PHASE GRID CONNECTED MODULAR MULTILEVEL CONVERTER” completed by **ELİF BEYHAN ÇERÇİ** under supervision of **PROF.DR. EYÜP AKPINAR** and we certify that in our opinion it is fully adequate, in scope and in quality, as a thesis for the degree of Master of Science.



Prof. Dr. Eyüp AKPINAR

Supervisor



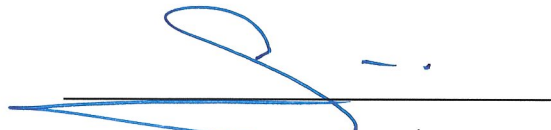
Doç. Dr. Murat BOZTEPE

(Jury Member)



Dr. Öğr. Üyesi Abdül Balıkcı

(Jury Member)



Prof. Dr. Kadriye ERTEKİN

Director
Graduate School of Natural and Applied Sciences

ACKNOWLEDGEMENT

I would like to express my special thanks to my supervisor, Prof. Dr. Eyüp Akpınar for his support, patience, encouragement and guidance throughout my graduate education.

Secondly, I would like to thank my parents, friends and especially my husband who helped me finalizing this project within limited time, for their encouragements and support

Elif BEYHAN ÇERÇİ

ANALYSIS AND CONTROL OF SINGLE-PHASE GRID CONNECTED MODULAR MULTILEVEL CONVERTER

ABSTRACT

The thesis focuses on mathematical analysis and control of modular multilevel converters. For transient and steady state analysis, the required mathematical model is constituted, open and closed loop working conditions are simulated on computer program. In these simulations, both energy and current control are built and analyzed separately to suppress circulating current. Additionally, the whole system is made independent from the real values by converting the system into per unit. In modular multilevel converters, the relationship between the suppressing the circulating current and the resonance condition formed by second harmonic current. The analytic calculation of the resonance frequency is compared with the simulation results.

Keyword : Modular multilevel converter, energy control, current control, circulating current, per – unit conversion, second harmonic, resonance frequency

TEK FAZ ŞEBEKE BAĞLANTILI MODÜLER ÇOK SEVİYELİ DÖNÜŞTÜRÜCÜ ANALİZ VE KONTROLÜ

ÖZ

Bu tez çalışması modüler çok seviyeli dönüştürücülerin matematiksel analizi ve kontrolü üzerinde yapılmıştır. Geçici ve kararlı durum analizleri için gerekli matematiksel model oluşturulmuş, açık ve kapalı çevirim çalışma koşulları bilgisayar ortamında simule edilmiştir. Bu simülasyonlarda dolaşım akımının bastırılması için enerji ve akım kontrolü ayrı ayrı kurgulanmış ve incelenmiştir. Ayrıca, tüm sistem birim-değerlere çevrilerek analiz edilmek suretiyle gerçek boyutlara bağlı olmaktan çıkarılmıştır. Modüler çok seviyeli dönüştürücülerde, ikinci harmonik akımına bağlı oluşan rezonansın ortadan kaldırılması için dolaşım akımının bastırılması ile olan bağlantısı incelenmiştir. Rezonans frekansının analitik hesaplanması simülasyon sonuçlarıyla karşılaştırılmıştır.

Anahtar kelimeler: Modüler çok seviyeli dönüştürücü, enerji kontrolü, akım kontrolü, dolaşım akımı, birim dönüşümü, ikinci harmonik, rezonans frekansı

CONTENTS

	Page
M.Sc THESIS EXAMINATION RESULT FORM	ii
ACKNOWLEDGEMENT	iii
ABSTRACT	iv
ÖZ	v
LIST OF FIGURES	viii
LIST OF TABLES	x
CHAPTER ONE - INTRODUCTION	1
1.1 Introduction	1
1.2 Objectives	5
1.3 Thesis Outline	6
CHAPTER TWO - MODULAR MULTILEVEL CONVERTERS	7
2.1 Description and Working Principles	7
2.2 Mathematical Model	10
2.3 Control Strategies	15
2.3.1 Modulation methods	15
2.3.1.1 Level Shifted PWM	15
2.3.1.1.1 Phase Disposition PWM	15
2.3.1.1.2 Phase oppositon dispotion PWM	16
2.3.1.1.3 Alternative phase opposition disposition PWM	17
2.3.1.2 Phase shifted PWM	18
2.3.1.3 Nearest level modulation	19
2.3.2 Inner Control	19
2.3.2.1 Sorting algorithms	19
2.3.2.2 Energy Control	20
2.3.2.3 Circulating current control	22
2.4 Arm Capacitance and Inductance Selection	22

CHAPTER THREE - MATLAB MODELS	28
3.1 Open Loop Control Model	28
3.1.1 Per Unit Model Conversion	33
3.2 Energy Control Model.....	34
3.3 Energy Control with Resonant Controller of Grid Current.....	40
3.4 Circulating Current Control with PR Controller	45
3.4.1 Optimization of PR parameters	47
3.4.2 Simulation Results	51
3.5 Comparison of Simulation Results of Four Different Analysis	52
3.6 Differential Current Analysis by Changing the Grid Frequency	56
CHAPTER FOUR - CONCLUSION	59
REFERENCES	60
APPENDICES	63

LIST OF FIGURES

	Page
Figure 1.1 Neutral point clamped (NPC)	2
Figure 1.2 Flying capacitor (FLC)	3
Figure 1.3 Cascaded Half Bridge MMC	4
Figure 2.1 MMC structure.....	8
Figure 2.2 Half Bridge submodule.....	9
Figure 2.3 Submodule current states	10
Figure 2.4 Phase disposition PWM for N+1 level	16
Figure 2.5 Phase opposition disposition PWM for 2N+1 level	17
Figure 2.6 Alternative phase opposition disposition PWM	18
Figure 2.7 Phase shifted PWM	18
Figure 2.8 Sorting algorithm scheme	20
Figure 2.9 Block diagram of circulating current control.....	22
Figure 3.1 The modulation signals for the upper and lower arms	28
Figure 3.2 The Simulink model of the MMC	30
Figure 3.3 (a) Open loop model differential current and (b) its steady-state variation	31
Figure 3.4 (a) Arm capacitor voltages and (b) its steady state.....	32
Figure 3.5 Upper and lower arm currents	33
Figure 3.6 Block diagram of energy controlled model	35
Figure 3.7 MATLAB Blocks of second model.....	36
Figure 3.8 Detailed control block of energy controller in MATLAB Simulation	37
Figure 3.9 (a) Circulating current, (b) steady state	37
Figure 3.10 Capacitor voltages	38
Figure 3.11 Sum of Energy, (W^{Σ})	39
Figure 3.12 Difference of energy, (W^{Δ})	39
Figure 3.13 Block diagram of energy controlled model with PR controller.....	40
Figure 3.14 The block diagram of the PR controller	40
Figure 3.15 Detailed control block of third model MATLAB Simulation	41
Figure 3.16 Output current reference, real and error graphs.....	42
Figure 3.17 Generated Output Voltage	43

Figure 3.18 Differential current (a) initial and (b) steady state.....	43
Figure 3.19 Total Energy of third model, (W^Σ)	44
Figure 3.20 Difference of energy, (W^Δ)	45
Figure 3.21 Differential current control part block diagram.....	45
Figure 3.22 Differential current control algorithm common part	46
Figure 3.23 FFT Window of circulating current controlled model.....	46
Figure 3.24 PR Controller	47
Figure 3.25 Initial points of controller parameters.....	47
Figure 3.26 Flowchart for the use of optimization toolbox	48
Figure 3.27 Bode Diagram.....	50
Figure 3.28 Generated Ki and Kp parameter for optimization	50
Figure 3.29 (a) Differential current and (b) its steady state	51
Figure 3.30 Capacitor voltages	52
Figure 3.31 Generated Output Voltage of Current controlled model	52
Figure 3.32 Differential current of open Loop model in per unit	53
Figure 3.33 Differential current of second model in per unit	54
Figure 3.34 Differential current of third model in per unit	54
Figure 3.35 Differential current of current controlled model in per unit	55
Figure 3.36 Change of differential current based on frequency in pu	57
Figure 3.37 Differential current behaviour in current controlled model depending on frequency (a) ripple (b) peak amplitude in per unit	58
Figure A.1 Inside of the first MATLAB block, calculation of the differential current	63
Figure A.2 Inside of the third MATLAB block, calculation of the arm voltages.....	63
Figure A.3 Second energy controlled model MATLAB blocks	64
Figure A.4 Inside of the energy calculation MATLAB block	65
Figure A.5 Second model control block	65
Figure A.6 Third model MATLAB blocks	66
Figure A.7 Third model control block	67
Figure A.8 Circulating current controlled model MATLAB blocks.....	68

LIST OF TABLES

	Page
Table 2.1 Coefficients and energy levels	26
Table 3.1 System parameters	29
Table 3.2 System parameters in per unit	34
Table 3.3 Third model system parameters	42



CHAPTER ONE

INTRODUCTION

1.1 Introduction

Energy demand is getting an increase with the growing population and development on the technology. As a result of that increasing demand, efficiency and reliability terms become vital. Thus, studies on power electronics increasingly continue gaining importance.

The economic and environmental sides of this energy need, enlarge the interest in renewable energy production. The place of production area is more dependent than the fossil fuel resources based facilities. Thus, the transmission of the generated electricity become a major problem to be solved. To reduce the power losses on transmission lines and power quality distortions, the power electronics based technology is needed. High voltage direct current (HVDC) and flexible alternative current transmission systems (FACTS) are some examples for the solution of the problems. Transmission over long distances by dealing with losses and quality problems, HVDC systems are becoming common and efficient. Limitation of short circuit current, lower losses and costs are some advantages of direct current (DC) transmission instead of alternative current (AC). The electricity generated in the utility may not be satisfying the desired features, the currents of the non-linear loads, the voltage or/and frequency may be different than must be. The active power filters and the static reactive power compensation systems are the other power electronic technologies for the solutions of power quality issues. The voltage source converters (VSC) based HVDC applications seems to be efficient and suitable structure due to its smaller size and filter requirements compared with line commutated converters.

The multilevel converters are the VSC which generates multilevel voltage waveforms at the AC side. Multilevel structures cause less harmonic at the output voltage and hence reduce the need of filter circuit. Also, by dividing the output voltage

into levels allows to generate higher voltages without facing any limitation problem of the semiconductors voltage ratings.

Firstly, the three-level neutral point clamped (NPC) inverter is proposed in 1979 (Nabae, Takashi & Akagi, 1979). It is mainly used in motor drive applications. Initially, rising the power rating and using in high power applications were aimed. However, its complexity of the switching and high installation cost due to high numbers of diodes used are the major drawbacks of the NPC. The five-level converter structure is given in figure 1.1. The dc link is divided into 5 levels by the capacitors having the voltage level of $V_{dc}/(n-1)$ where n is the number of voltage level.

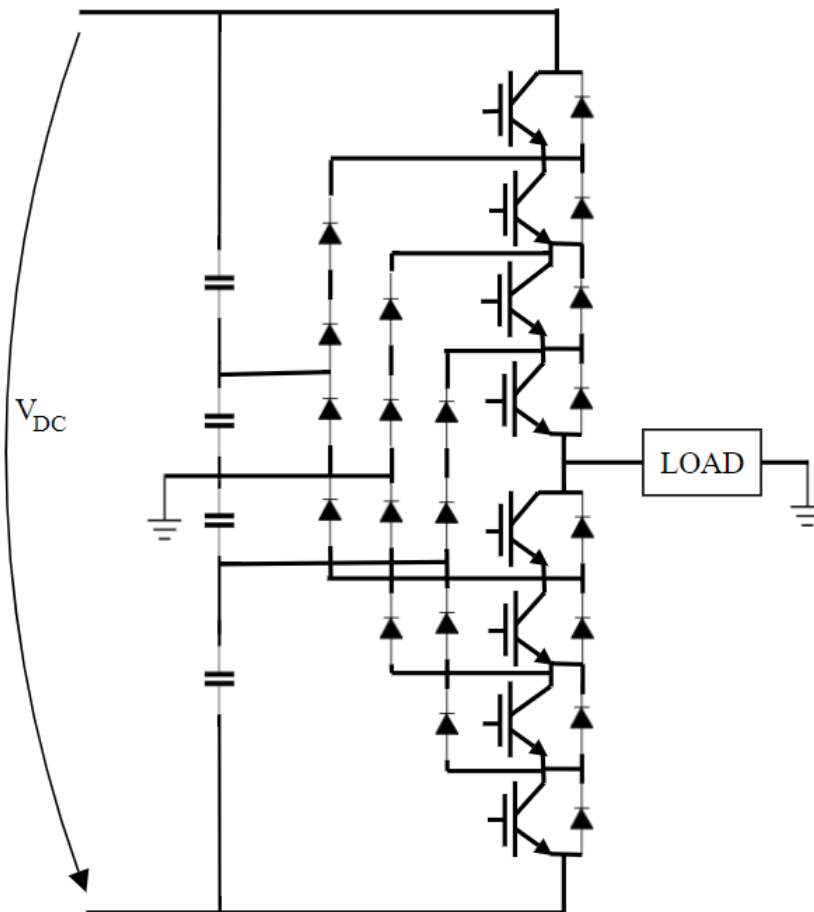


Figure 1.1 Neutral point clamped (NPC)

In 1992, the second topology that is the three-level flying capacitor (FLC) is proposed (Meynard & Foch, 1992). It is named as capacitor clamped inverter. The topology is similar with the diode-clamped structure but the capacitors are used instead of diodes. The sizing, complexity and cost are the major disadvantages of the circuit.

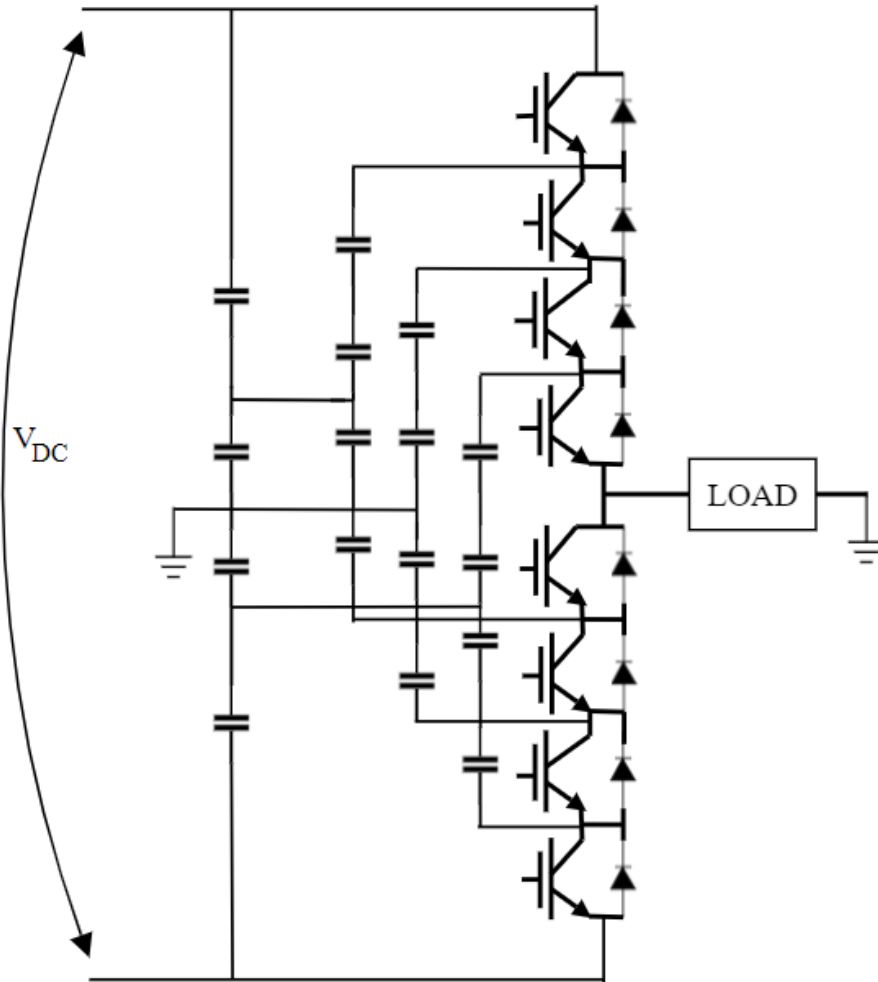


Figure 1.2 Flying capacitor (FLC)

Lastly, the cascaded half bridge was proposed in motor drive application by Robicon (Hammond, 1997) in 1997. Then, the circuit configuration in figure 1.3 was presented. This converter (MMC) is proposed by Lesnicar and Marquardt (Marquardt & Lesnicar, 2003) in 2003. The current research on the modular structure is mainly focused on this topology with different submodules. Half bridge is one of the submodule among the many others.

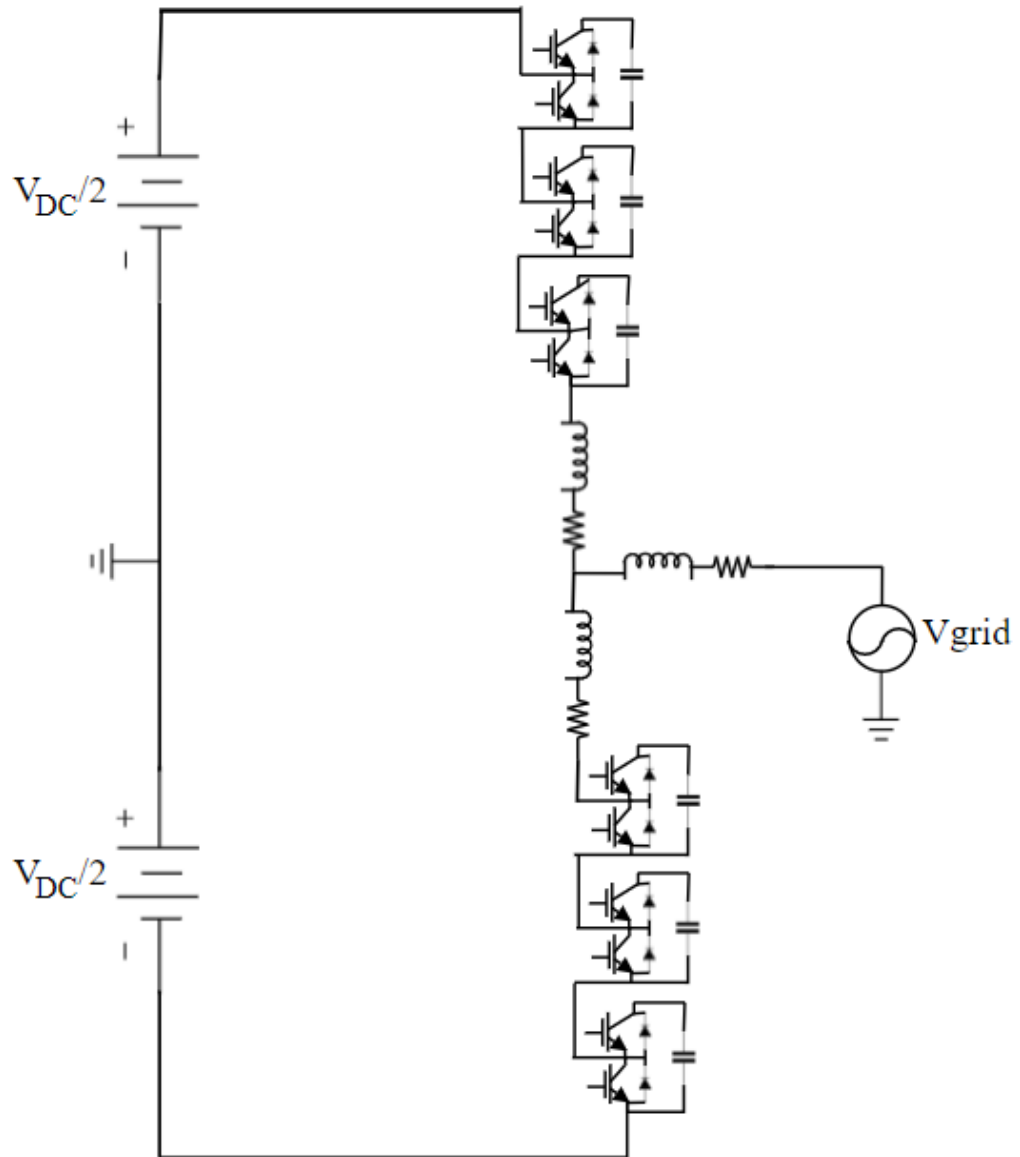


Figure 1.3 Cascaded Half Bridge MMC

The modular multilevel converters (MMC) has an important impact on the design of AC/DC conversion in high power applications. It is implemented in the manufacturing process easily in last decade due to its modular structure and many other advantages (Asimakopoulos, 2013) like a low voltage rated solid state devices and electromechanical components are used in cascade structure. In order to obtain the ideal rectification features, the optimizing control algorithms, some sorting algorithms (Glinka & Marquardt, 2003) and PWM modulations techniques are suggested by (Hagiwara, Maeda & Akagi, 2011).

The advantages can be summarized as;

- Smaller voltage steps at the output meant that more sinusoidal waveform and less harmonic distortion. Also, stepped output reduce the dv/dt rate (voltage change) and decrease the electromagnetic compatibility (EMC) problems.
- Modular structure allows easily increase the power and voltage ratings of the system by adding new submodules or in a failure protect the system by changing the module which has fault.
- MMCs can be controlled by the lower switching frequencies than the conventional two or three level VSC. This reduce the switching losses.

There are only two main disadvantages. These are; the initial costs due to the large number of semiconductors and the circuit elements. And the other is the complex control needed on the voltage balancing of the capacitors and switching of the solid state devices.

1.2 Objectives

This thesis focus on the control techniques to suppress the circulating current of MMC and the effects of circulating current on resonance condition. The grid connected MMC is simulated in MATLAB by using the per unit system.

The main objectives of this thesis are;

- i. Analyzing the main operation principles and the mathematical model of MMC.
- ii. Studying control methods of MMC.
- iii. Analyzing and comparing the results of these methods.
- iv. Analyzing the effect of circulating current on resonance frequency.

1.3 Thesis Outline

The average value model of the MMC is presented in (Jinke, et al., 2018), (Antonopoulos, Angquist & Nee, 2009) and (Teodorescu & Zarri, 2012). This model is converted to the per unit in this paper in order to specify the inductance and capacitor values independent to power rating of the converter. The resonance frequency is analyzed by depending on the circulating current harmonics in (Ilves, Antonopoulos, Norgga & Nee, 2012). The study in (Ilves et al., 2014) is used for the selection of arm inductance and submodule capacitance based on the power capacity of converter and resonance frequency.

This thesis mainly focus on the effect of the circulating current and the its suppressing methods. In chapter 2, the operation principle is examined in detail, some of the submodule structures are investigated and the control algorithms are discussed.

Chapter 3, the open loop energy control is analyzed, the energy control with proportional resonant controller and differential current control algorithms are used in the MATLAB simulations. Mathematical models are updated in per unit (pu) and results are compared.

Chapter 4, the effect of circulating current at resonance frequency is examined. Open loop operation and inner current control methods are evaluated whereas the grid frequency is changed from 5 Hz to 70 Hz to see the response of the currents including the resonance condition.

Finally, the thesis covers the conclusion with the comparison of simulation results.

CHAPTER TWO

MODULAR MULTILEVEL CONVERTERS

2.1 Description and Working Principles

The modular multilevel converters consist of numbers of submodules (SM). Each leg has two arms called as upper and lower arms. Each arms has N number of submodules. This number is determined depending on the submodule voltage rating and the voltage rating of the converter. The number of submodules in the upper and lower arms in each phase leg must be equal. Its modular structure allows to increase or decrease the number of modules for critical loads in a faulty condition.

All arms also have a small inductance and the internal resistance of it that have the significant effect for limiting the circulating current. The selection of these parameters are depending on the instantaneous power balance in the specified range of capacitor voltage ripple and the constraint on the resonance frequency (Ilves, Antonopoulos, Norgga, Harnfors & Nee, 2014).

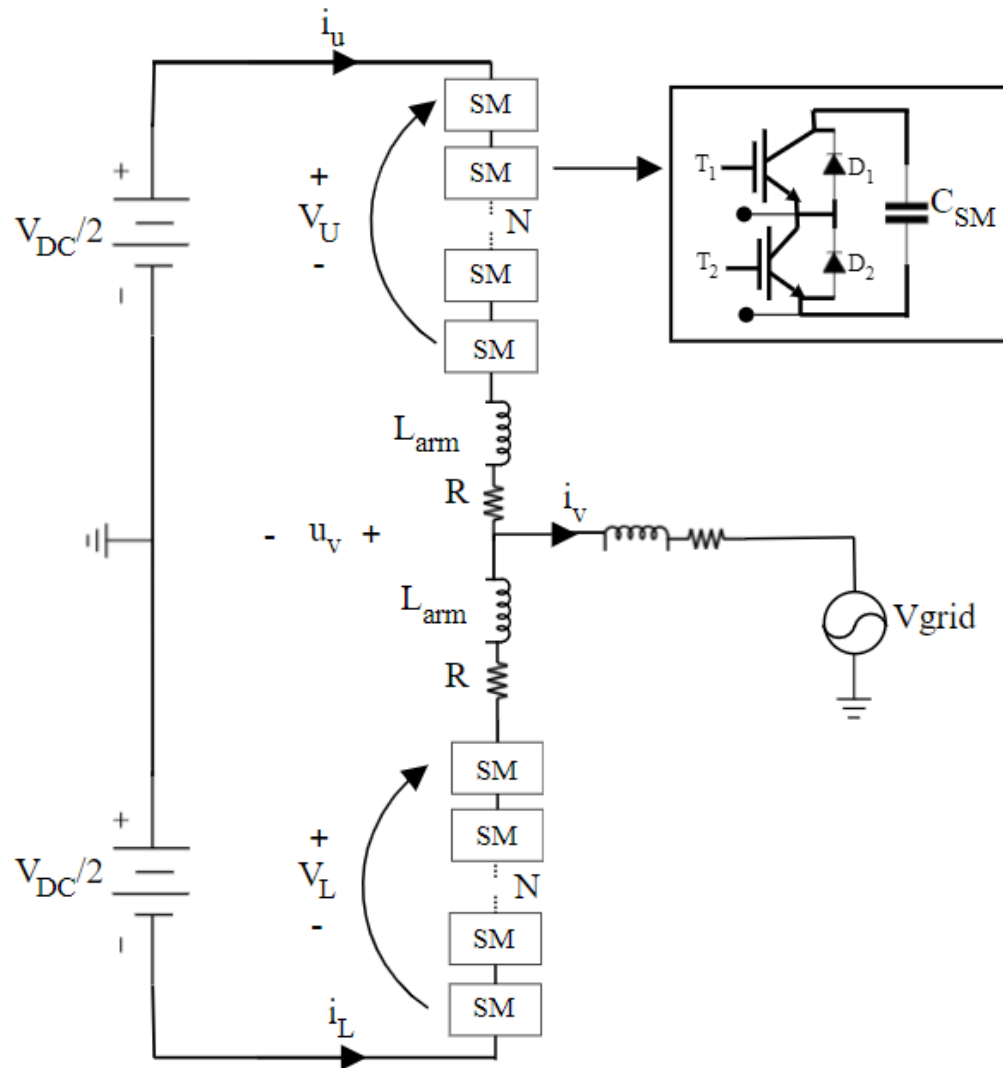


Figure 2.1 MMC structure

In this thesis, a half bridge (HB) topology shown in figure 2.1 is taken into account as a submodule structure. The HB structure is one of the commonly used topologies in the MMCs. The half bridge submodule consists of two IGBT switches, two anti-parallel diodes and one capacitor that is connected in parallel to the solid state devices as shown in the figure 2.2.

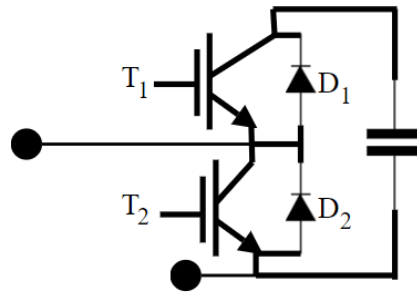


Figure 2.2 Half Bridge submodule

DC-link capacitors behaves like a voltage source. In the operation of the converter, some of them are inserted and the others are bypassed in order to generate desired voltage level. Transistors T1 and T2 work in a complementary mode, while one is on the other is off and they never conduct simultaneously to avoid the short circuit across the capacitor. The pulse width modulation technique can be applied by keeping enough amount of dead time between T1 and T2.

The capacitor voltage changes according to the direction of the current and the decisions on the selection of the switching status are made in order to keep the voltage variation across the capacitor in the specified range. There are four possible switching status as it is shown in figure 2.3. (Glinka & Marquardt, 2005)

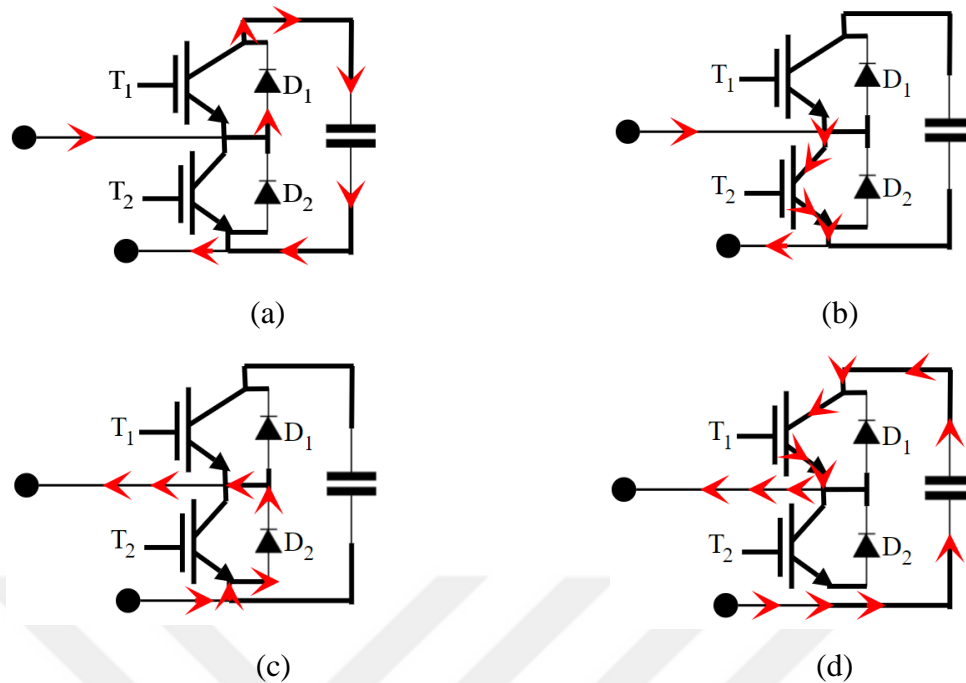


Figure 2.3 Submodule current states

For two current direction possibilities, control algorithm selects the SMs which will be charged or discharged. In mode (a) situation, T1 is on and T2 is off. The positive current directly flows through the capacitor and it will be charged. In modes (b) and (c) condition, the SM is bypassed. In mode (d), T1 is on and T2 is off, the negative current flows the paths seen in the figure and discharge the capacitor. In either direction of the current, the charge in the capacitor can be controlled, hence the voltage level across the capacitor is controlled.

2.2 Mathematical Model

The converter has N submodules in each arm and the capacitance value in each submodules is C_{SM} . Before starting modelling the system parameters N number should be selected according to consideration of;

- The output voltage waveform,
- Total harmonic distortion,
- DC side voltage level

- Semiconductors voltage and current limitations and
- Cost

Technically, the most important criteria is the output voltage waveform and total harmonic distortion (THD) level. When the number of modules is increased, the output voltage waveform approaches to ideal sinusoidal wave. Submodule capacitor voltage level becomes V_{DC}/N and that level must be kept under the semiconductors voltage ratings. Thus, for the operation with the high voltage DC the number of submodule can be increased to keep the SM voltages under available voltage ratings of the solid state devices in the market.

The equivalent capacitor of the series connected modules can be defined as follows.

$$C_{Arm} = \frac{C_{SM}}{N} \quad (2.1)$$

The arm effective capacitance depends on modulation (insertion) index m ;

$$n_U = \frac{1}{2}(1 - m \sin(\omega t)) \quad (2.2)$$

$$n_L = \frac{1}{2}(1 + m \sin(\omega t)) \quad (2.3)$$

$$C_{eff.} = \frac{C_{Arm}}{n(t)} \quad (2.4)$$

Insertion index specifies the number of inserted capacitors or in the equivalent form of submodules. $n(t)=1$ means that all modules in the arm are inserted, while all modules are bypassed when $n(t)=0$. The upper and lower arm modulation indexes are related to the output voltage waveform. The model used in this study assumes that the output voltage is pure sinusoidal wave, hence n_U and n_L can be generated from the equations (2.2) and (2.3). Equal voltage regulation is ensured by this selection method.

According to current direction and capacitance values, this mechanism works. If current direction is on charging way, the lowest charged submodule will be inserted and the highest will be bypassed. For the opposite way, the highest charged capacitor will be inserted and the others are bypassed.

All control algorithms aim to set all capacitor voltages equal. Thus, assuming that they are equally charged as V_{CU} and V_{CL} which are the upper and lower arm capacitor voltage levels, respectively. Then the inserted voltage by the arm becomes sum of all active submodules' voltages and it is expressed as;

$$V_U = n_U V_{CU}^{\Sigma} \quad (2.5)$$

$$V_L = n_L V_{CL}^{\Sigma} \quad (2.6)$$

For the one phase leg, shown in the figure 2.1, the sum of upper and lower arm currents is equal to the output current. The difference of upper and lower arm currents is the circulating current i_{diff} . It has the priority for control strategy of the converter.

$$i_v = i_U + i_L \quad (2.7)$$

$$i_{diff} = \frac{i_U - i_L}{2} \quad (2.8)$$

$$i_U = \frac{i_v}{2} + i_{diff} \quad (2.9)$$

$$i_L = \frac{i_v}{2} - i_{diff} \quad (2.10)$$

The currents are related in terms of the equivalent capacitor voltages as follows;

$$i_U = \frac{C_{Arm} d(V_{CU}^{\Sigma})}{n_U dt} \quad (2.11)$$

$$i_L = \frac{C_{Arm} d(V_{CL}^\Sigma)}{n_L dt} \quad (2.12)$$

The equations (2.9)-(2.12) are used to obtain differential equations for upper and lower arm voltages as follows;

$$\frac{d(V_{CU}^\Sigma)}{dt} = \frac{n_u}{C_{Arm}} i_{diff} + \frac{n_u}{2C_{Arm}} i_v \quad (2.13)$$

$$\frac{d(V_{CL}^\Sigma)}{dt} = \frac{n_L}{C_{Arm}} i_{diff} - \frac{n_L}{2C_{Arm}} i_v \quad (2.14)$$

The upper and lower current can be expressed as follows;

$$i_U = I_{DC} + \frac{I_M}{2} \sin(\omega t) + I_{diff} \sin(2\omega t) \quad (2.15)$$

$$i_L = -I_{DC} + \frac{I_M}{2} \sin(\omega t) - I_{diff} \sin(2\omega t) \quad (2.16)$$

The mathematical model can be simplified by using Kirchhoff's law by using figure 2.1.

$$V_{DC}/2 - V_U - L_{arm} \frac{di_U}{dt} - Ri_U = u_v \quad (2.17)$$

$$-V_{DC}/2 + V_L - L_{arm} \frac{di_L}{dt} - Ri_L = u_v \quad (2.18)$$

Subtracting equation (2.18) from equation (2.17);

$$V_{DC} - (V_U + V_L) = L_{arm} \frac{d}{dt} (i_U - i_L) + R(i_U - i_L) \quad (2.19)$$

If the equation (2.8) is substitute into (2.19);

$$V_{DC} - (V_U + V_L) = 2L_{arm} \frac{di_{diff}}{dt} + 2Ri_{diff} \quad (2.20)$$

$$V_{diff} = L_{arm} \frac{di_{diff}}{dt} + Ri_{diff} \quad (2.21)$$

$$\frac{V_{DC}}{2} - U_V - V_{diff} = V_U \quad (2.22)$$

$$\frac{V_{DC}}{2} + U_V - V_{diff} = V_L \quad (2.23)$$

The dynamic model of the converter is obtained as follows,

$$\frac{d}{dt} \begin{bmatrix} i_{diff} \\ V_{CU}^\Sigma \\ V_{CL}^\Sigma \end{bmatrix} = \begin{bmatrix} -\frac{R}{L_{arm}} & -\frac{n_u}{2L_{arm}} & -\frac{n_L}{2L_{arm}} \\ \frac{n_u}{C_{arm}} & 0 & 0 \\ \frac{n_L}{C_{arm}} & 0 & 0 \end{bmatrix} \begin{bmatrix} i_{diff} \\ V_{CU}^\Sigma \\ V_{CL}^\Sigma \end{bmatrix} + \begin{bmatrix} \frac{V_{DC}}{2L_{arm}} \\ \frac{n_u i_v}{2C_{arm}} \\ -\frac{n_L i_v}{2C_{arm}} \end{bmatrix} \quad (2.24)$$

$$\dot{x} = Ax + u \quad (2.25)$$

As it can be clearly observed from the third order state space equation, x is the state variables vector and u is the input parameters vector. n_u and n_L are varying in time periodically (Harnefors, et al. 2013).

2.3 Control Strategies

2.3.1 Modulation methods

The pulse width modulation (PWM) technique is most commonly used method to control AC to DC power converters. Comparison of triangular wave with sinusoidal reference generates the control signal which contains 1s and 0s in time domain. The level-shifted and phase-shifted PWM methods can be used in the control of MMC. Additionally, nearest level modulation is also a very useful method for these converters to keep submodule voltages equally.

2.3.1.1 Level Shifted PWM

This method is formed of N triangular carrier wave with f_c carrier frequency which equals to switching frequency f_s for $N+1$ switching. However, when we consider $2N+1$ level the f_c became as an half of f_s . We can group them into 3 branches which are phase disposition (PD), phase opposition disposition (POD), alternative phase opposition disposition (APOD).

2.3.1.1.1 Phase Disposition PWM. The principles of PD-PWM is mainly discussed at (Holmes D. G. & Lipo T. A. 2003). The number of carriers directly depends on number of SMs per arm of MMC.

All carriers that are used for one arm, have no phase difference. Their voltage level decides the inserted submodule. For $N+1$ level, the 180° phase difference between upper and lower arm carriers is required. Figure 2.4 shows the phase disposition.

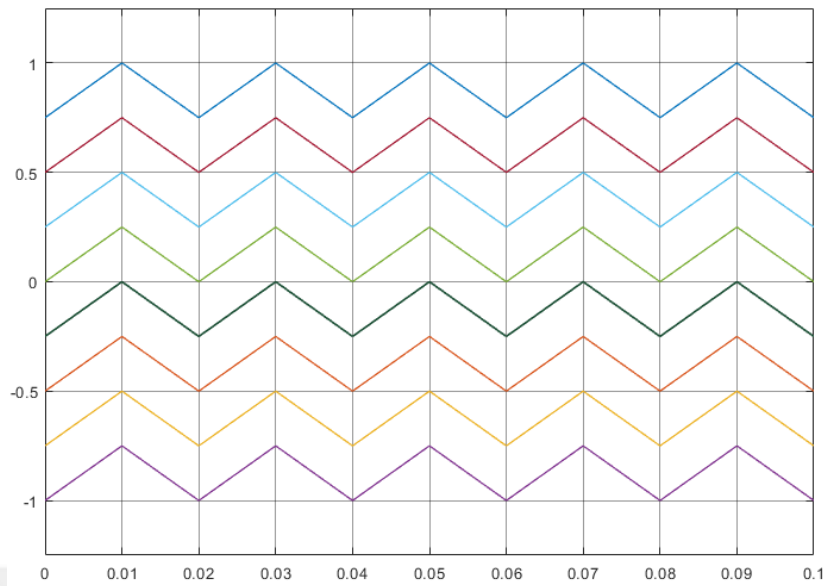


Figure 2.4 Phase disposition PWM for N+1 level

There are two options for the output level. For N+1 level as above two sets of carriers must be used to control. Otherwise, for 2N+1 level one set is enough. Each set includes N identical carrier with the amplitude of V_{dc}/N and displaced between the range of 0 to V_{dc} .

2.3.1.1.2 Phase oppositon dispotion PWM. In this method N-1 carriers are used. The carriers above the zero are in phase and the others below the zero reference shifted 180°.

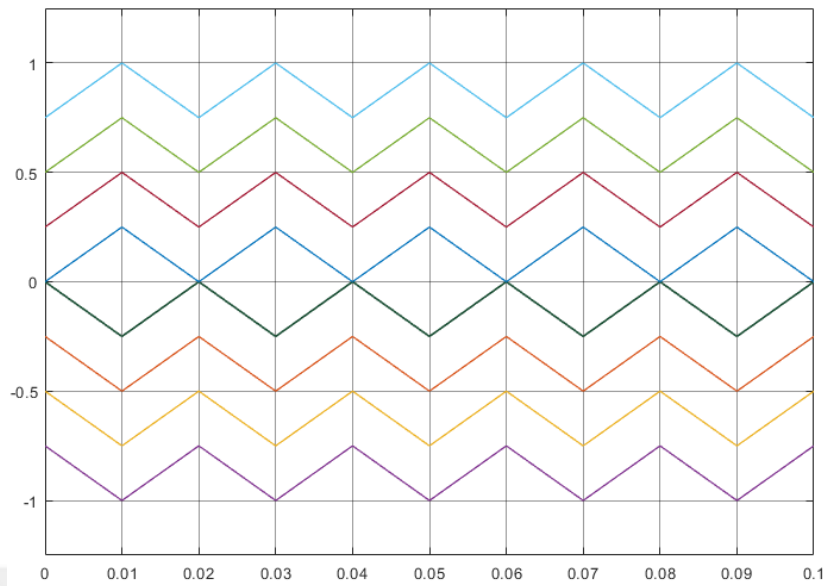


Figure 2.5 Phase opposition disposition PWM for $2N+1$ level

2.3.1.1.3 Alternative phase opposition disposition PWM. In this modulation technique, each carrier in a set has 180° degree phase difference with its adjacent. For example, if the first carrier is considered as a reference, the second one needs to be placed at 180° phase and third one become again 0° and so on. Figure 2.6 shows the alternative phase opposition disposition PWM.

For level difference, in $N+1$ condition, upper and lower arm sets have 180° difference. Means that if upper arm's first carrier at 0° then lower arm's become at 180° . However, if there is no phase difference, it generates $2N+1$ levels.

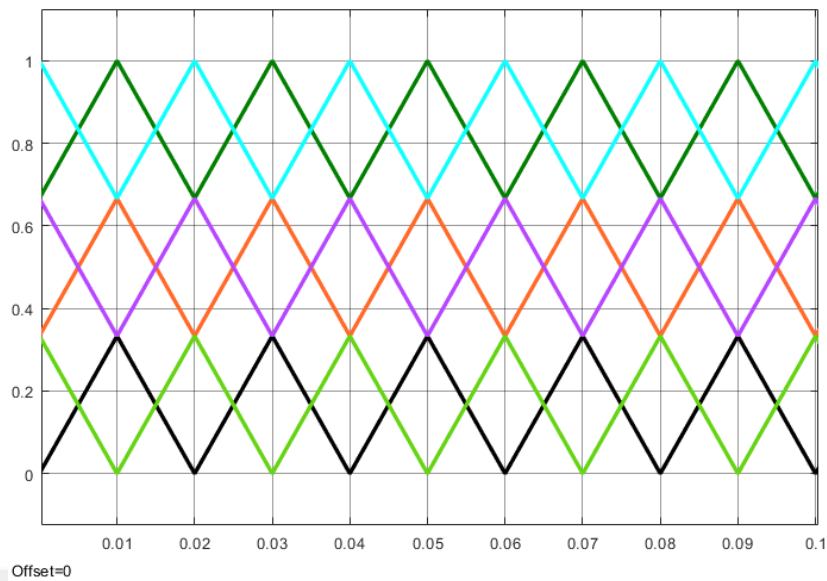


Figure 2.6 Alternative phase opposition disposition PWM

2.3.1.2 Phase shifted PWM

This method also needs N identical triangular carriers as the previous modulation methods. However, in PS-PWM their peak to peak levels are same, each triangular wave is displaced by an angle of $360^\circ/N$. Figure 2.7 shows the carrier waves for the phase shifted PWM.

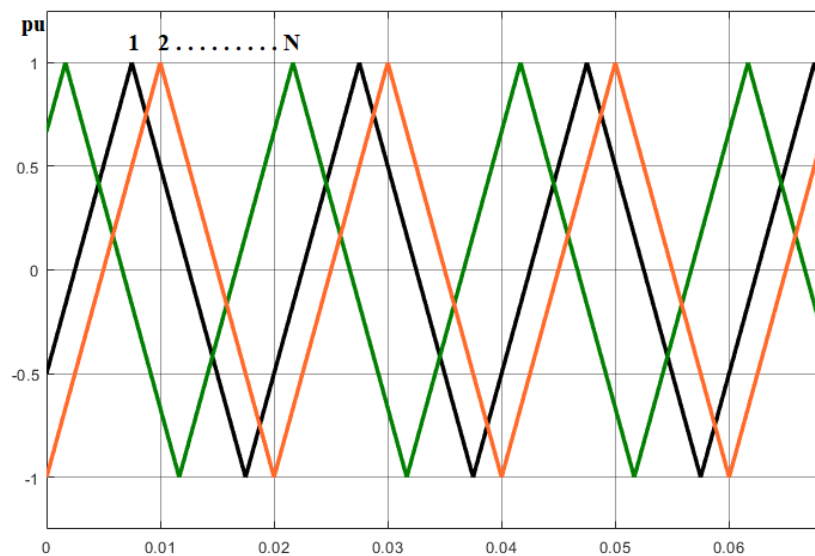


Figure 2.7 Phase shifted PWM

By configuring the phase difference, it is possible to get $N+1$ and $2N+1$ voltage level as an output of converter. While, placing $180^\circ/N$ phase difference between upper and lower arm carriers generates $2N+1$ level output, controlling the converter with same carrier set for both arm results $N+1$ level.

2.3.1.3 Nearest Level Modulation

Nearest level modulation is based on selection of the right module by comparing voltage difference between the reference voltage and the actual voltage levels and inserts the most proper modules. The direction of the current is the key point for deciding on the discharging or charging capacitor condition as mentioned in section 2.1. This method aims to eliminate circulating current and harmonic orders by keeping all submodule voltages at the desired level. There are no need for carrier waves, hence more feasible for the systems which have high number of submodules.

2.3.2 Inner Control

Such a control methods aim to increase the efficiency of the converter and eliminate the harmonic components of circulating current. There are several approaches studied, three out of them are examined below. The first one is sorting algorithms. This method is based on the selection of right module to equalize the submodule voltages (Marquardt & Lescinar, 2003).

2.3.2.1 Sorting Algorithms

Sorting and select algorithm control measures and sorts the capacitor voltages into a sequence, highest to lowest or in the other way. Then it selects the required modules according to current direction. As mentioned at previous sections, current direction is directly related with charging and discharging conditions of the submodule capacitors. Thus, if positive current is flowing, the algorithm selects the lowest level modules to increase their voltage level and create equalized system. In the other option, for

negative current, highest level modules are selected to discharge the capacitor voltage. Figure 2.8 shows the flowchart for the sorting algorithm.

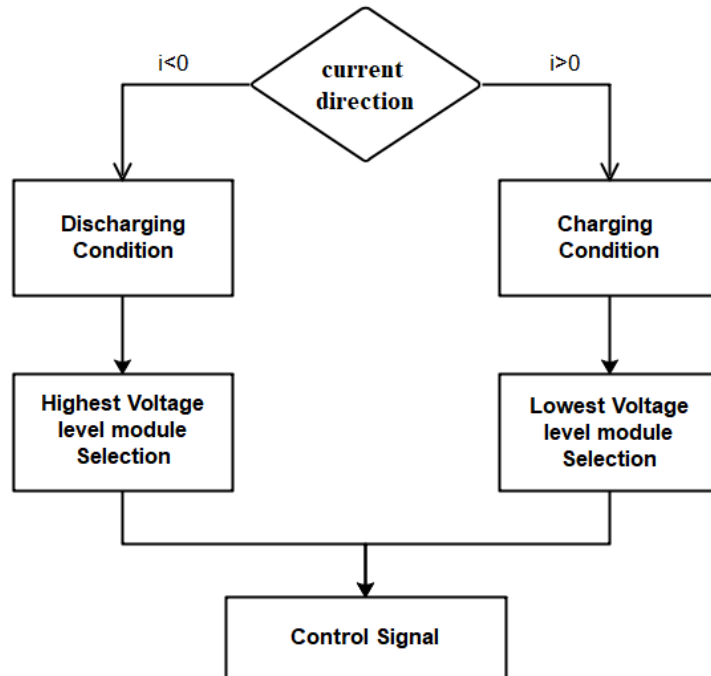


Figure 2.8 Sorting algorithm scheme

This algorithm aims to balance arm submodule voltages and suppress the circulating current which occurs from these unbalanced voltage levels.

2.3.2.2 Energy Control

The total active power is generated by dc part of the circulating current. However, due to the nature of submodule capacitors some fluctuation occurs and this generates the AC part of this current which is totally loss. As a consequence of the active power supplied by the DC part of the dc link current, the AC part circulates in the converter and has the effect on the converter efficiency. So, the AC (circulating current) component must be eliminated.

According to equation (2.20), the circulating current only depends on the instantaneous sum of upper and lower arm voltages. If it is assumed that the stored energy due to these voltages equally shared between modules. The energy equations become;

$$W_{CU} = \frac{1}{2} C_{Arm} (V_{CU})^2 \quad (2.26)$$

$$W_{CL} = \frac{1}{2} C_{Arm} (V_{CL})^2 \quad (2.27)$$

It is possible to write instantaneous power equations for the upper and lower arms of the same leg as follows;

$$\frac{dW_{CU}}{dt} = i_u V_U \quad (2.28)$$

$$\frac{dW_{CL}}{dt} = i_L V_L \quad (2.29)$$

The total and difference energy can be written as follows;

$$W_C^\Sigma = W_{CL} + W_{CU} \quad (2.30)$$

$$W_C^\Delta = W_{CU} - W_{CL} \quad (2.31)$$

These equations can be used to relate the instantaneous powers we convert the upper equations into power form and re-write informs of (2.28) and (2.29) by putting equation (2.9) and (2.10) it yields,

$$\frac{dW_C^\Sigma}{dt} = (V_{dc} - 2V_{diff}) i_{diff} - e_v i_v \quad (2.32)$$

$$\frac{dW_C^\Delta}{dt} = \left(\frac{V_{dc}}{2} - V_{diff}\right) i_v - 2e_v i_{diff} \quad (2.33)$$

The total energy control is directly related with i_{diff} and its dc part. $V_{dc} i_{diff}$ represents the instantaneous input power to the converter from the dc link, $V_{diff} i_{diff}$ is the loss due the arm impedance and $e_v i_v$ is the instantaneous output power. e_v and i_v do not contain the dc components. The ac component of i_{diff} can be used to control the balance between upper and lower arm energy flow, because the average value of the right hand side of equation (2.30) is zero.

2.3.2.3 Circulating current control

In this control method, the main purpose is to eliminate the ac component of the circulating current. i_{diff} is generated from the upper and lower arm currents via equation (2.8). The low-pass filter can be used to obtain pure dc component of the difference current. The only ac part remains after subtracting the dc component produced by the filter from the whole current. In the second stage of the controller, the actual ac part can be compared to the reference (that is expected to be zero) and passed through the proportional resonant (PR) current controller. This control method shown in figure 2.9 is analyzed in (Wang et al., 2017) and (Jinke et al., 2018).

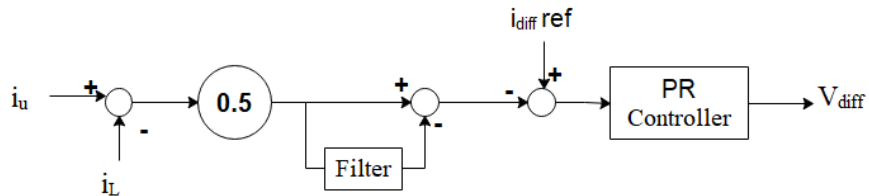


Figure 2.9 Block diagram of circulating current control

2.4 Arm Capacitance and Inductance Selection

Capacitors in the submodules need consideration to minimize voltage ripples. The voltage ripples may not be totally eliminated however, a suitable capacitance selection can minimize it. A high capacitance value suppresses the ripples but this increases the cost unnecessarily. Thus, in order to find an optimum value of C, the minimum energy needs and the relation between this need and capacitance must be determined (Ilves et al., 2014)

The energy stored in a submodule is;

$$e_{SM} = \frac{1}{2} C_{SM} V_{SM}^2 \quad (2.34)$$

The coefficient k_{dc} is the rate of submodule voltage and the dc voltage and its nominal value is 1;

$$V_{SM} = k_{dc} \frac{V_{DC}}{N} \quad (2.35)$$

The arm has N submodules so the nominal energy stored in the arm capacitor is N times of (2.34). It must be noted that while the submodule energy is indicated by "e", the arm energy is shown by using capital letter E;

$$E_{arm} = \frac{N}{2} C_{SM} V_{SM}^2 \quad (2.36)$$

By using the equation (2.35),

$$E_{arm} = \frac{C_{SM}}{2N} k_{dc}^2 V_{DC}^2 \quad (2.37)$$

The peak voltage across the capacitor can be limited to the rated voltage. For this reason, k_{max} indicates the upper limit of the submodule instantaneous voltage.

$$v_{SM} = k_{max} \frac{V_{dc}}{N} \quad (2.38)$$

$$e_{SM} \leq \frac{1}{2} C_{SM} \left(k_{max} \frac{V_{DC}}{N} \right)^2 \quad (2.39)$$

Then maximum energy stored in the submodule is obtained as follows;

$$e_{\max} = \frac{1}{2} C_{SM} \left(k_{\max} \frac{V_{DC}}{N} \right)^2 \quad (2.40)$$

$$e_{\max} = \frac{C_{arm}}{2} k_{\max}^2 V_{DC}^2 \quad (2.41)$$

Let us define,

$$E_{\max} = \frac{C_{arm}}{2} k_{\max}^2 V_{DC}^2 \quad (2.42)$$

The difference between E_{arm} and E_{\max} gives the maximum excess energy stored in each arm,

$$\Delta E_{\max} = E_{\max} - E_{arm} \quad (2.43)$$

$$\Delta E_{\max} = \frac{C_{SM}}{2N} k_{\max}^2 V_{DC}^2 - \frac{C_{SM}}{2N} k_{dc}^2 V_{DC}^2 \quad (2.44)$$

$$\Delta E_{\max} = \frac{C_{SM}}{2N} V_{DC}^2 (k_{\max}^2 - k_{dc}^2) \quad (2.45)$$

$$C_{\min} = \frac{2N \Delta E_{\max}}{V_{DC}^2 (k_{\max}^2 - k_{dc}^2)} \quad (2.46)$$

C_{\min} is the minimum submodule capacitance. Voltage ripples can be minimized by using larger SM capacitors. It also controls the circulating current and reduce the impact of its harmonic components to the system. However, larger size capacitors are costly and increases the area needed for the system. Thus, it is usually preferred to retain the size of the capacitor minimum and suppressed the circulating current via control algorithm.

Thus, the nominal energy stored in each arm is,

$$E_{nom} \geq \frac{\Delta E_{max}}{k_{max}^2 - k_{dc}^2} \quad (2.46)$$

Substituting C_{min} into (2.39), E_{max} becomes,

$$E_{max} \geq \frac{k_{max}^2}{k_{max}^2 - k_{dc}^2} \Delta E_{max} \quad (2.47)$$

The equation (2.47) shows that the minimum energy requirement of the system depends on the maximum amount of excess energy and constant k_{max} and k_{dc} .

The instantaneous power and energy can be calculated from the upper and lower arm voltages V_U and V_L and the arm currents i_u and i_L . The instantaneous power in the upper arm capacitor is

$$p_u = V_U i_u \quad (2.48)$$

The energy stored on the capacitor is

$$e_U = \int p_u dt \quad (2.49)$$

The instantaneous power in the lower arm capacitor is

$$p_L = V_L i_L \quad (2.50)$$

The energy stored on the capacitor is

$$e_L = \int p_L dt \quad (2.51)$$

The peak values of e_U and e_L can be used as the maximum capacity of the energy storage ΔE_{\max} for both upper and lower arm. It should be noted that this peak value is the same for the minimization of circulating current. Thus,

$$\Delta E_{\max} = \max(e_U) \quad (2.52)$$

The coefficients and energy levels used in equation above are given in table 2.1;

Table 2.1 Coefficients and energy levels

K_{\max}	1.005
K_{dc}	0.998
E_U nominal	99.62
E_U maximum	101.1
ΔE_{\max}	1.48

When the coefficients and energy values in table 2.1 are used the minimum capacitance value for the arm is evaluated as 4.924 mF, for this system it is selected as 5 mF.

For the estimation of arm inductance, the resonance frequency limits according to minimum calculated capacitance value can be used. The value of inductance is effective on the limitation of the circulating current. The resonance frequency is

$$\omega_r = \sqrt{\frac{N}{L_{arm} C_{SM}}} \sqrt{\frac{2(n^2 - 1) + m^2 n^2}{8n^2 (n^2 - 1)}} \quad (2.53)$$

The highest resonant frequency is generated when modulation index (m) is equal to 1 and the second harmonic (n=2) is selected. The grid frequency should be greater than the highest resonance frequency for safe operation.

$$L_{arm} C_{SM} > \frac{5N}{48\omega^2} \quad (2.54)$$

The minimum value of the arm inductance can be obtained from (2.54). In this study, the value of arm inductance should be above 0.2 mH.



CHAPTER THREE

MATLAB MODELS

3.1 Open Loop Control Model

The model is firstly presented in (Ängquist et. al., 2010) and (Ängquist et. al., 2011) and mainly based on some assumptions that a perfect voltage sharing and capacitor insertion mechanism works properly as in proposed (Glinka & Marquardt, 2005). It is assumed that the lowest submodule is selected during the positive current circulation through the capacitors and charged to the reference level, otherwise the capacitor with the highest voltage level is discharged and this sequence is worked perfectly and continuously as in (Antonopoulos, Ängquist & Nee, 2009).

The model given in (2.24) for the open loop operation can be used to obtain the circulating current, the upper and lower arm voltages. This basic model gives the insight on the parameters of circulating current and operation of the converter without considering voltage balancing of the capacitors. The continuous variation of the capacitors with the perfect balance voltage is the basic assumption in the model. On this basis, the modulation indexes given in (2.2) for upper arm and (2.3) for the lower arm are used in the simulation. The modulation signals shown in figure 3.1 have the unity for maximum.

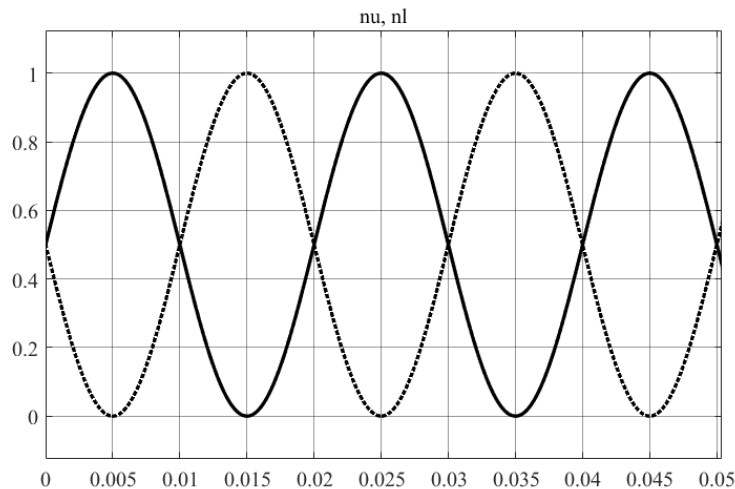


Figure 3.1 The modulation signals for the upper and lower arms

The system parameters used are listed Table 3.1.

Table 3.1 System parameters

I_v	$10 \sin (\omega t + \phi)$
f	50 Hz
ϕ	0
V_{DC}	200 V
C_{arm}	5 mF
L	3 mH
R	0.1Ω

The figure 3.2 shows the outline of the MATLAB simulation and constructed to solve the mathematical model. The first block and third block evaluates the differential current and arm voltages by solving the differential equation in (2.24). The details of these blocks also illustrated in the appendix. For solving these nonlinear set of equations, ode4 (Runge – Kutta) is selected as a solver in MATLAB with step size of 10^{-5} .

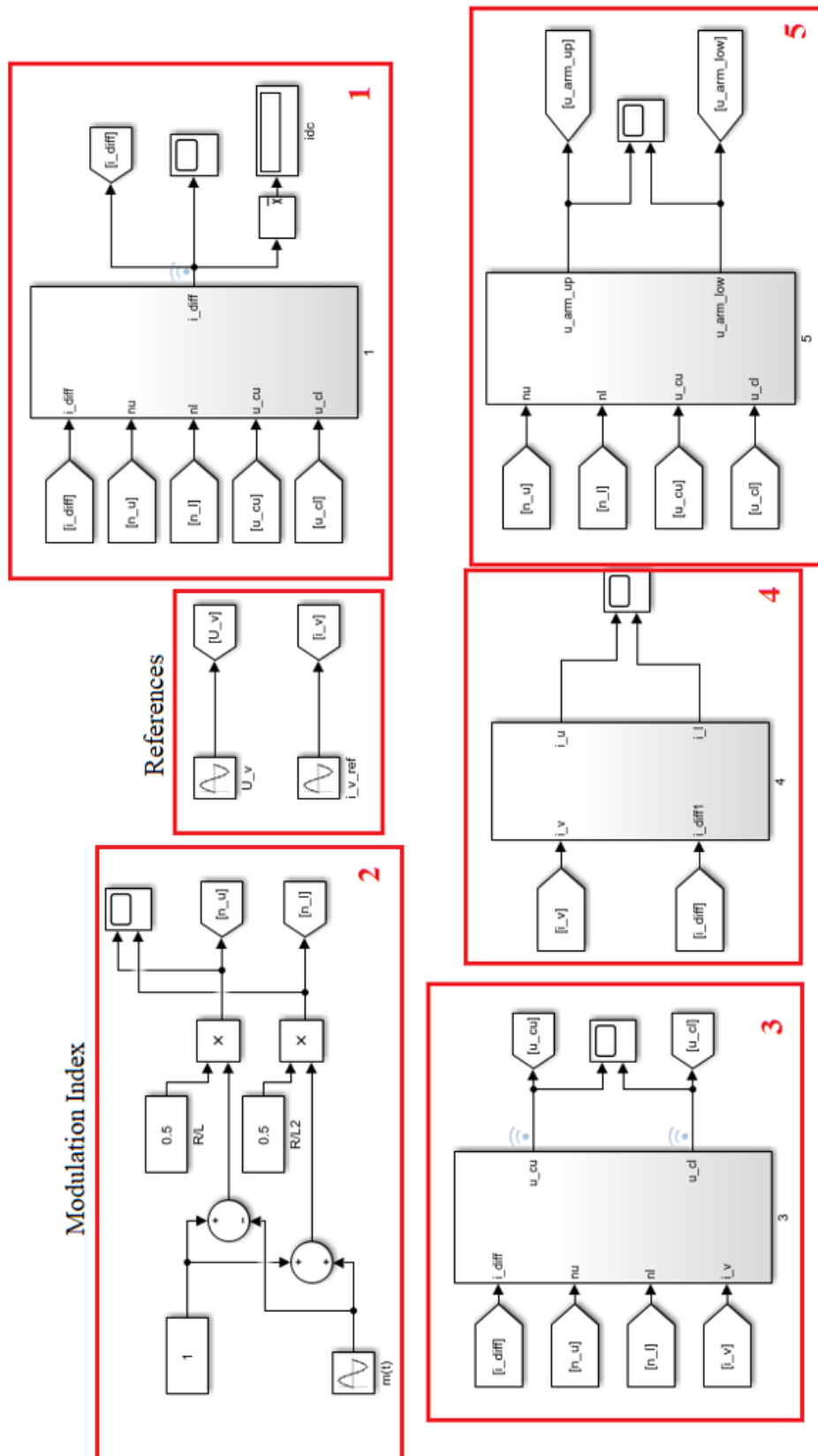
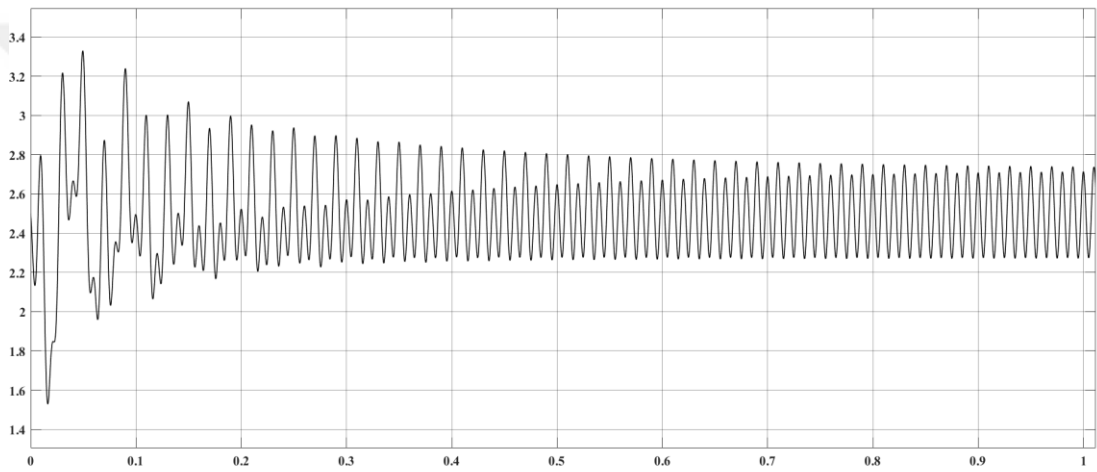
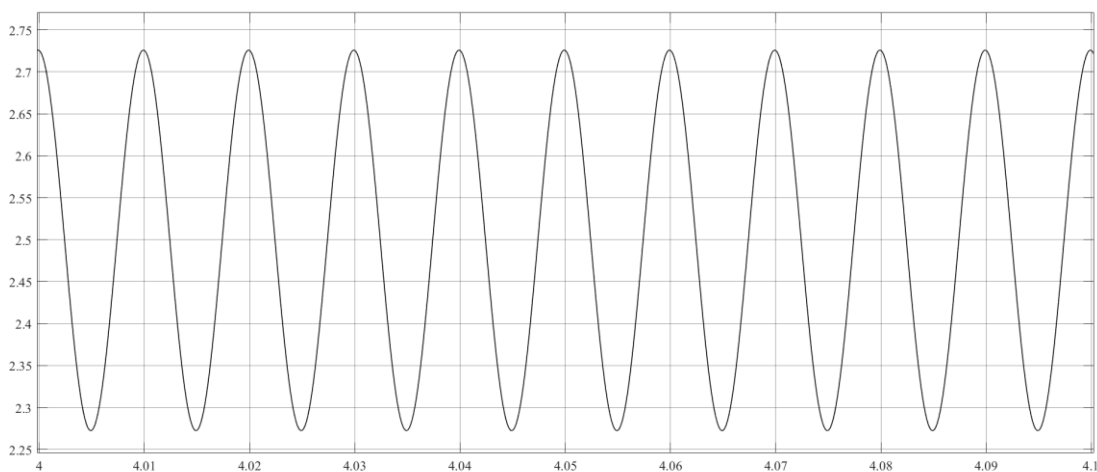


Figure 3.2. The Simulink model of the MMC

As seen from the figures, the steady state values for the circulating current, upper and lower arm voltages are specified by the inputs namely, the output AC current, modulation index and the DC link voltage level. The system settles down to these steady state operating point after the starting transients elapsed. The peak to peak value of the circulating current is around 0.5 A whereas the AC output current is set to the peak value of 10 A, it is almost 2.5 % of the inverter output current. The average value of the circulating current is almost 2.5 A. It should be noted that the inverter output current is the input to the model but the load voltage is not specified.



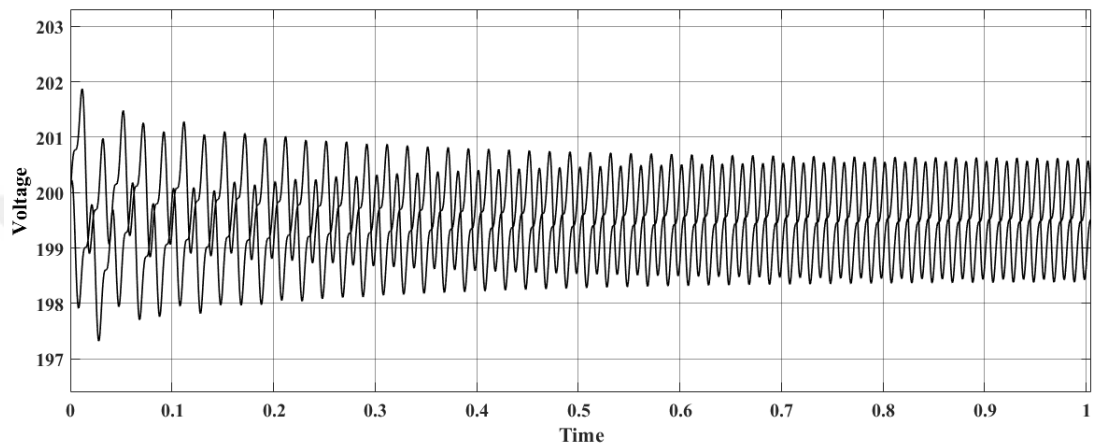
(a)



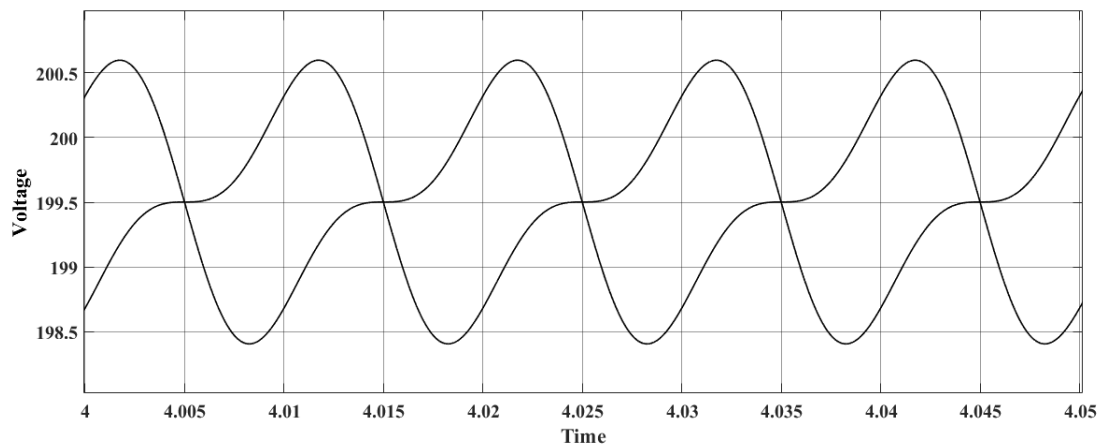
(b)

Figure 3.2 (a) Open loop model differential current and (b) its steady-state variation

The upper and lower capacitor voltages has the fluctuation around 4 V whereas the average of the capacitor voltage is around 199.5 V. The ripple is around % 2 even though the capacitor variations are continuous and the modulation changes with a pure sinusoidal form. The ripple has fundamental and second harmonic components. When the second harmonic in the circulating current is suppressed, the ripple component of the capacitor voltage will also be reduced.



(a)



(b)

Figure 3.3 (a) Arm capacitor voltages and (b) its steady state

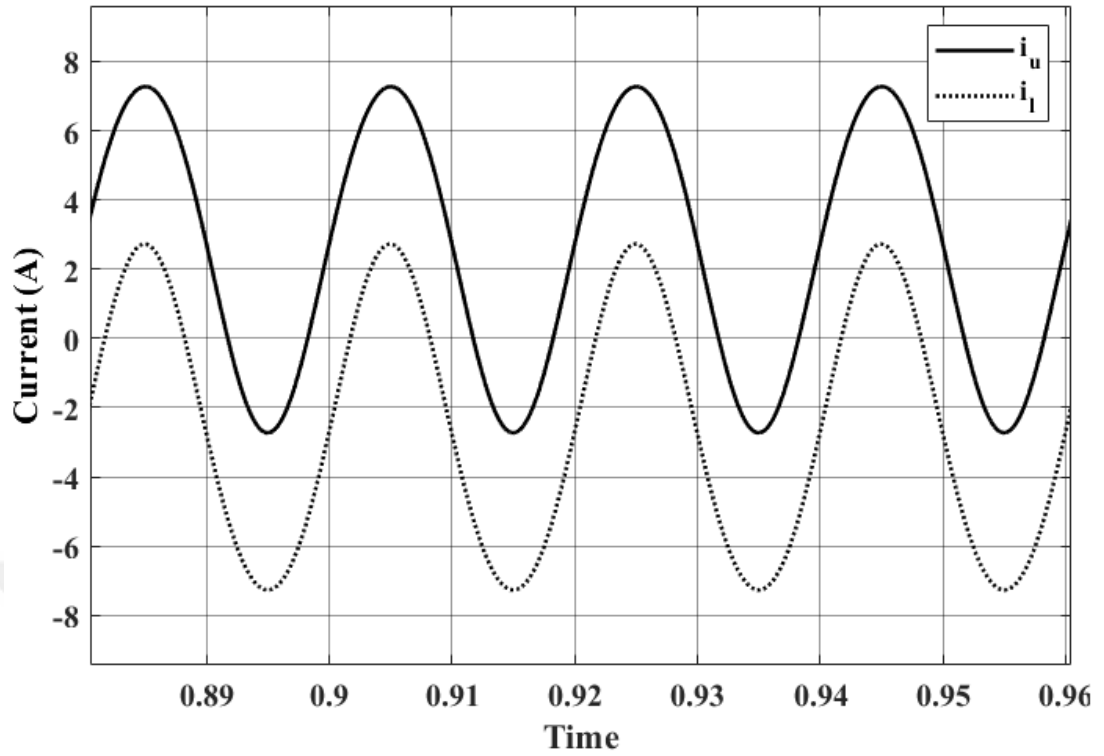


Figure 3.4 Upper and lower arm currents

3.1.1 Per Unit Model Conversion

The per unit system generates a mathematical model and simulation that are independent to the converter voltage, current and power ratings. The rated values of the converter output voltage (50V) and current (10A) are selected base values. These values are selected independently. The base values for the power and impedance are computed using the voltage and current base values as follows.

$$V_{base} = U_V \quad (3.1)$$

$$I_{base} = I_V \quad (3.2)$$

$$S_{base} = V_{base} I_{base} \quad (3.3)$$

$$Z_{base} = V_{base} / I_{base} \quad (3.4)$$

The per unit values of resistance, inductance and capacitor are computed from their actual values and base value of impedance as follows:

$$R_{pu} = \frac{R}{Z_{base}} \quad (3.5)$$

$$L_{pu} = \frac{L}{Z_{base}} \quad (3.6)$$

$$C_{pu} = C \cdot Z_{base} \quad (3.7)$$

Table 3.2 System parameters in per unit

V _{dc}	4 pu
R _{pu}	0.02 pu
L _{pu}	0.0006 pu
C _{pu}	0.025 pu

This per unit conversion will be implemented on all models to obtain parameter independent results and the calculated parameters given in table 3.2 are used.

3.2 Energy Control Model

The second systems is based on dynamic model given (2.24). The output current and voltage are taken into account as the reference values. The logic is basically controlling overall energy to balance capacitor voltages and suppress the circulating current. Firstly, the sum and difference of the energy errors are evaluated. The reference value for the total energy is calculated from the stored energy in the capacitors as follows:

$$W_C^\Sigma = 0.005 \times 200^2 = 200J \quad (3.8)$$

The reference for the difference of the upper and lower arm energies is set to zero for creating the balanced arm voltages. Energy is used as the control parameter in this structure. The control scheme is obtained as indicated below;

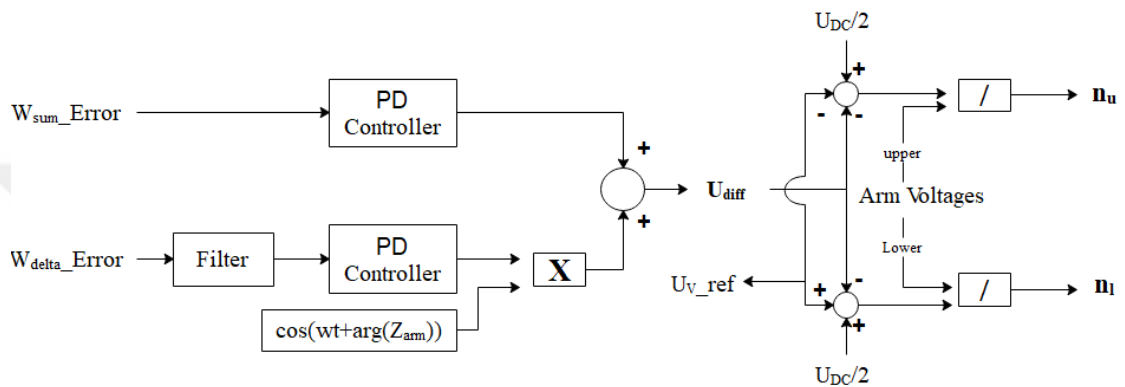


Figure 3.5 Block diagram of energy controlled model

Proportional derivative (PD) controllers are used both for energy difference and summation error evaluations. Inverter output current and voltage are taken into account from their reference values of 10A and 50V defined as the peak values.

The total energy is controlled by DC component of the differential current as it is seen from the equation (2.32) where i_{diff} is multiplied with V_{dc} . Thus, the dc part of the differential current is the dominant component. And the ac part is used to balance upper and lower arm energies.

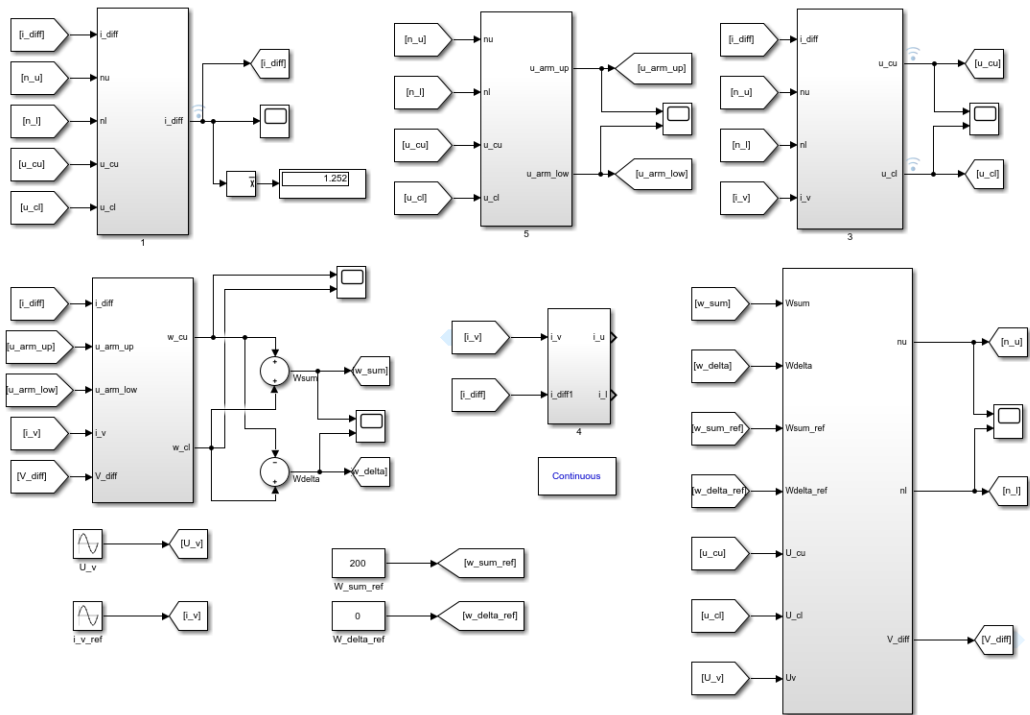


Figure 3.6 MATLAB Blocks of second model

1st, 3rd and the 5th blocks contain the open loop model. Energy is computed in the energy block, inside of this block is given in the appendix, and these data is the input for the control block shown in figure 3.8. PD controller aims to eliminate the error between the references and the actual values of the energies.

In the difference of the energy, a low pass filter is used to make the signal more stable and smooth. Then multiplied with the carrier wave which is at frequency of the output voltage and the carrier wave is shifted by the impedance angle created from the arm resistance and arm inductance.

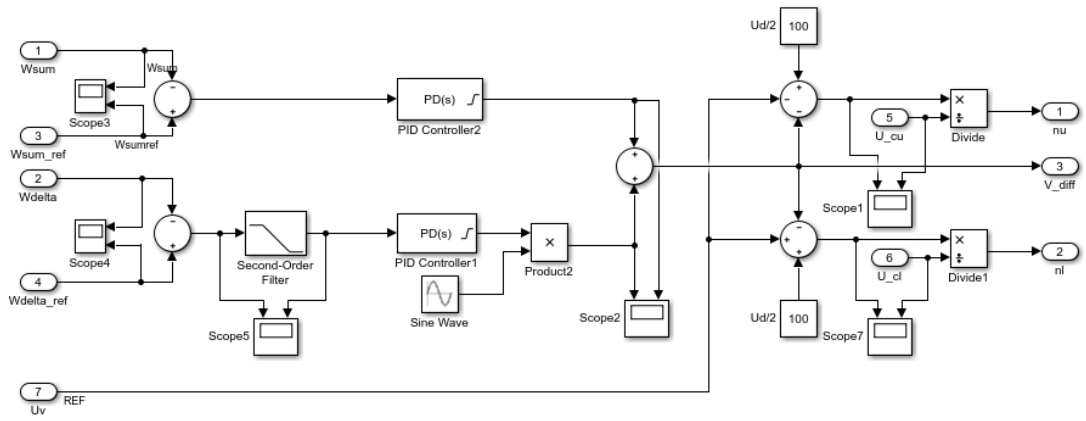
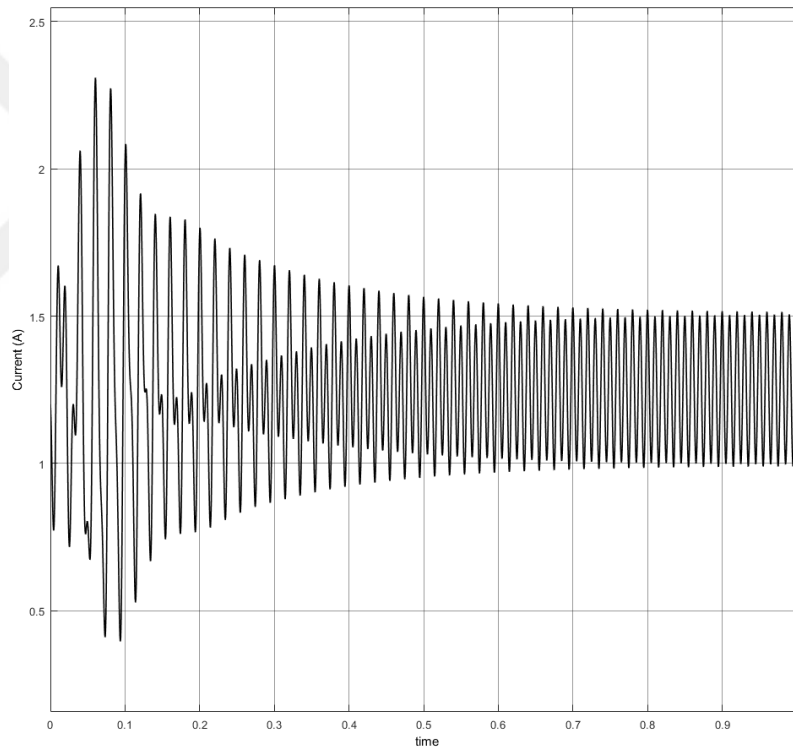
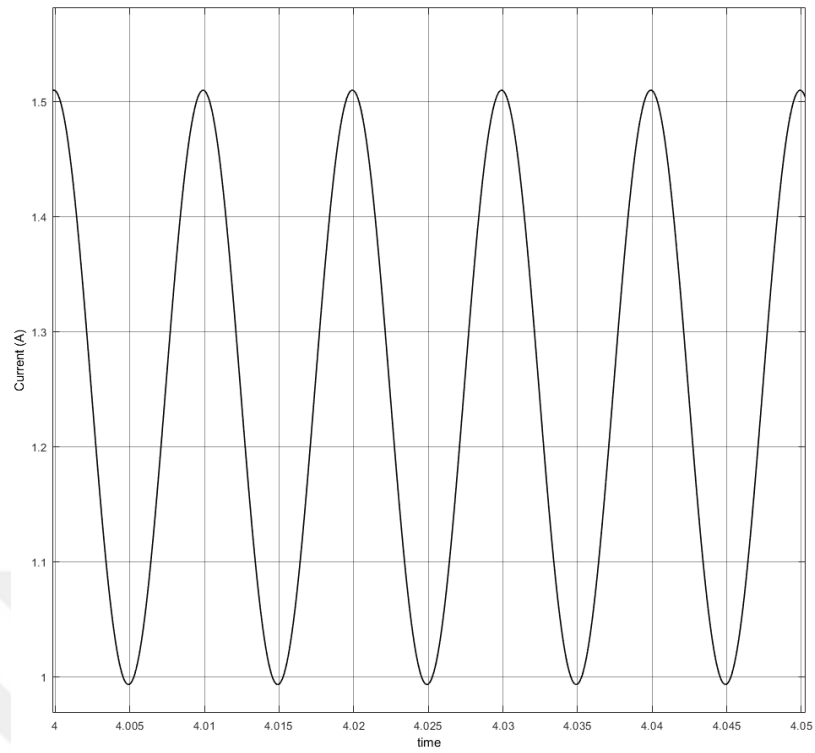


Figure 3. 7 Detailed control block of energy controller in MATLAB Simulation



(a)

Figure 3.8 (a) Circulating current, (b) steady state



(b)

Figure 3.9 continues

Figure 3.9 shows that such a limited control helps to decrease the settling period and the maximum overshoots in circulating current but the ripple to ripple magnitude of it is almost same as the value of open loop control.

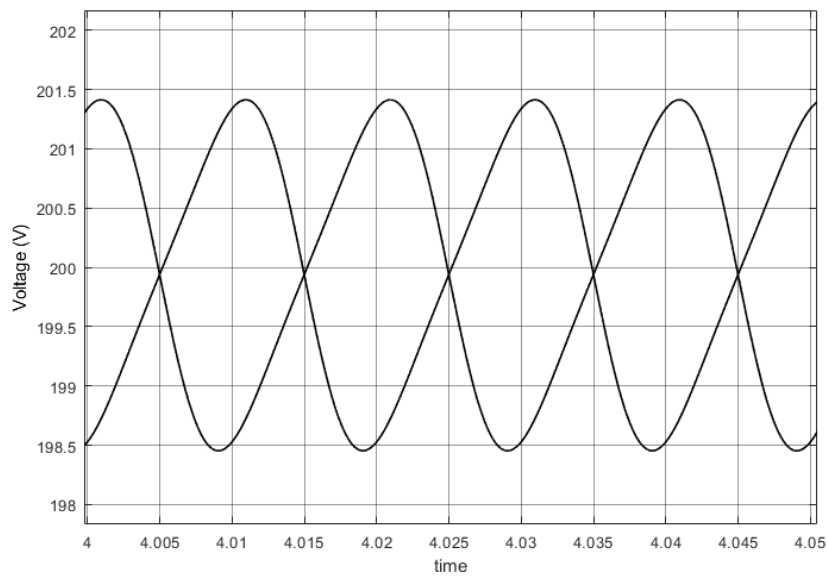


Figure 3.10 Capacitor voltages

Figure 3.10 shows that the arm total capacitor voltage settles down to the DC link voltage (200 V) as it is expected. The reference value of total energy as shown in figure 3.11 assures the operating point of this steady-state value.

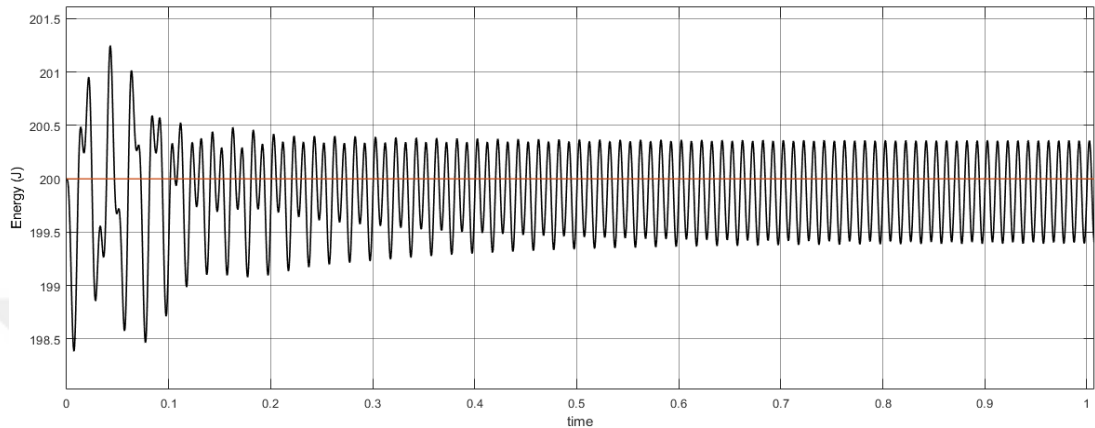


Figure 3.11 Sum of Energy, (W^2)

The total energy stored in the capacitors of upper and lower arms reaches at the reference value after a some amount of transient. The magnitude of oscillation is less than 1% at steady state and its frequency is 100 Hz as it is expected.

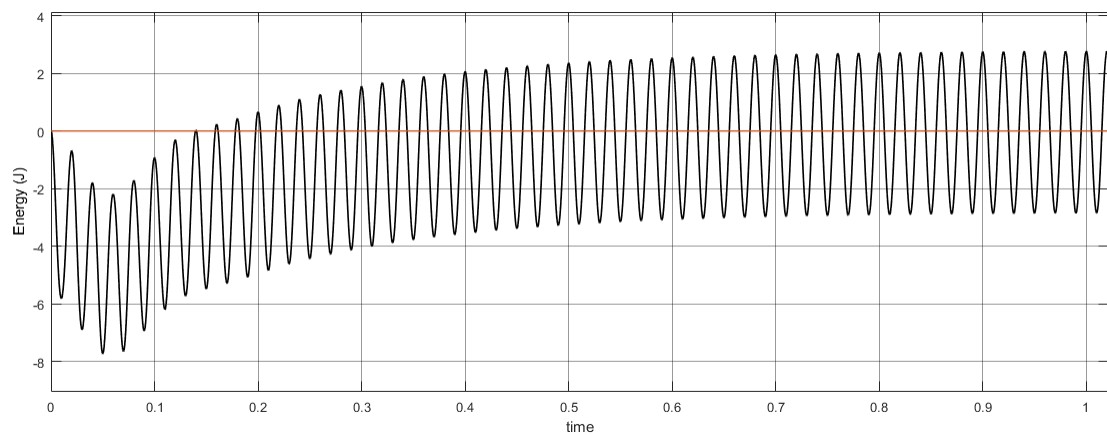


Figure 3.12 Difference of energy, (W^2)

The difference energy between the upper and lower arms, which occurs from the undesired inequality of the arm voltages, also settles down to the reference value (zero). The steady-state oscillation has the frequency of 50 Hz.

3.3 Energy Control with Resonant Controller of Grid Current

The third model shown in figure 3.13 is also based on the energy control model but in this part of the study the grid is connected to the inverter with the current controller. The first and second parts includes the same equations and the algorithm. Output current control is added in the third block which contains proportional resonance (PR) controller additionally. Output of the PR is used as the voltage reference to obtain the modulation indexes. The algorithm scheme is as illustrated in figure 3.14.

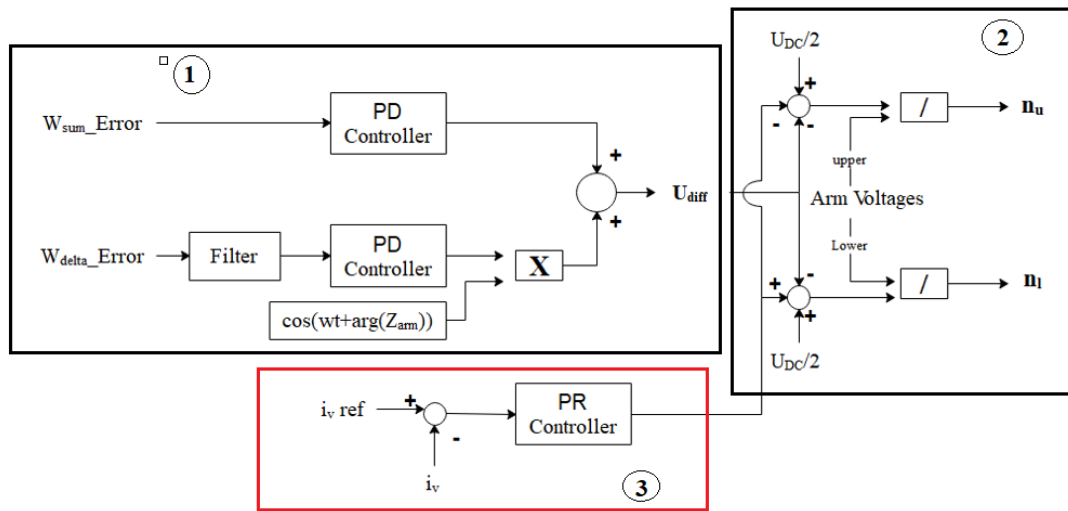


Figure 3.13 Block diagram of energy controlled model with PR controller

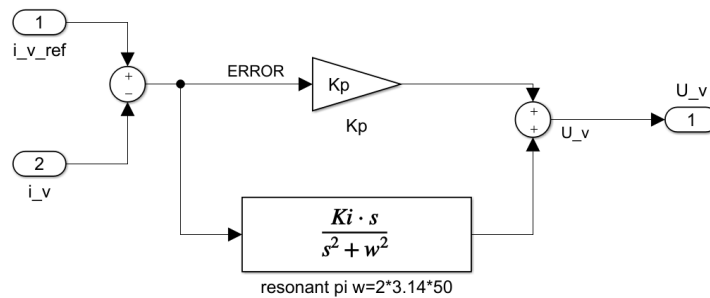


Figure 3.14 The block diagram of the PR controller

PR controller consists of two part, one is proportional part, K_p , which determines the system dynamics, and the other is resonance part, K_i . These parameter is selected via the optimization toolbox of the MATLAB (see section 3.4.1). Implementing a PR controller can eliminate the steady-state error via its very high gain at the resonance frequency, ideal PR controllers provide an infinite gain at selected frequency (Teoderescu & Liserre & Rodriguez, 2011) that is the grid frequency selected in this application. The ideal PR controller without the damping factor has the transfer function as follows (Teoderescu & Blaabjerg & Liserre & Loh, 2006):

$$G_{PR} = K_p + \frac{K_i s}{s^2 + \omega_0^2} \quad (3.9)$$

The simulation model prepared in the MATLAB is given in figure 3.15. In this analysis, the grid is considered as the power sink. The parameters of the simulation is given in Table 3.3.

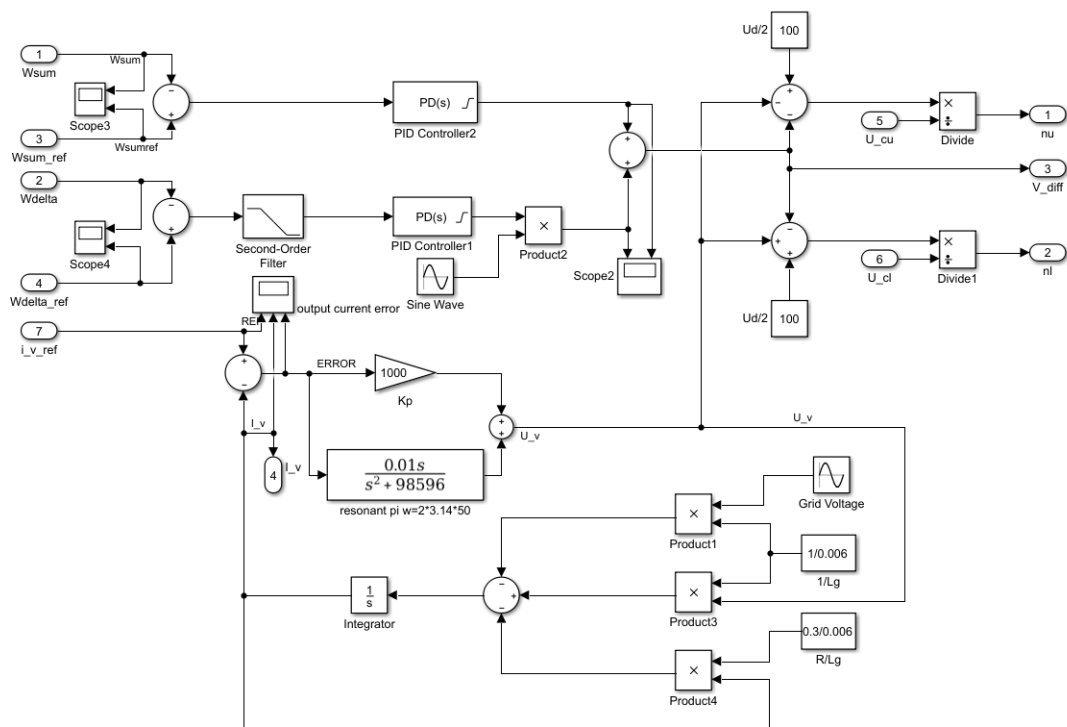


Figure 3.15 Detailed control block of third model MATLAB Simulation

Table 3.3 Third model system parameters

$W_{\text{sum_ref}}$	200
$W_{\text{delta_ref}}$	0
f	50 Hz
ϕ	0
V_{DC}	200 V
C_{arm}	5 mF
L	3 mH
R	0.1 Ω
R_g	0.3 Ω
L_g	6 mH
V_g	50 sin(wt)

By using PR controller for the output current, the reference current is tracked and the error between actual and reference currents is forced to zero. The simulation results in figure 3.16 are given for the actual current and its error due to the reference.

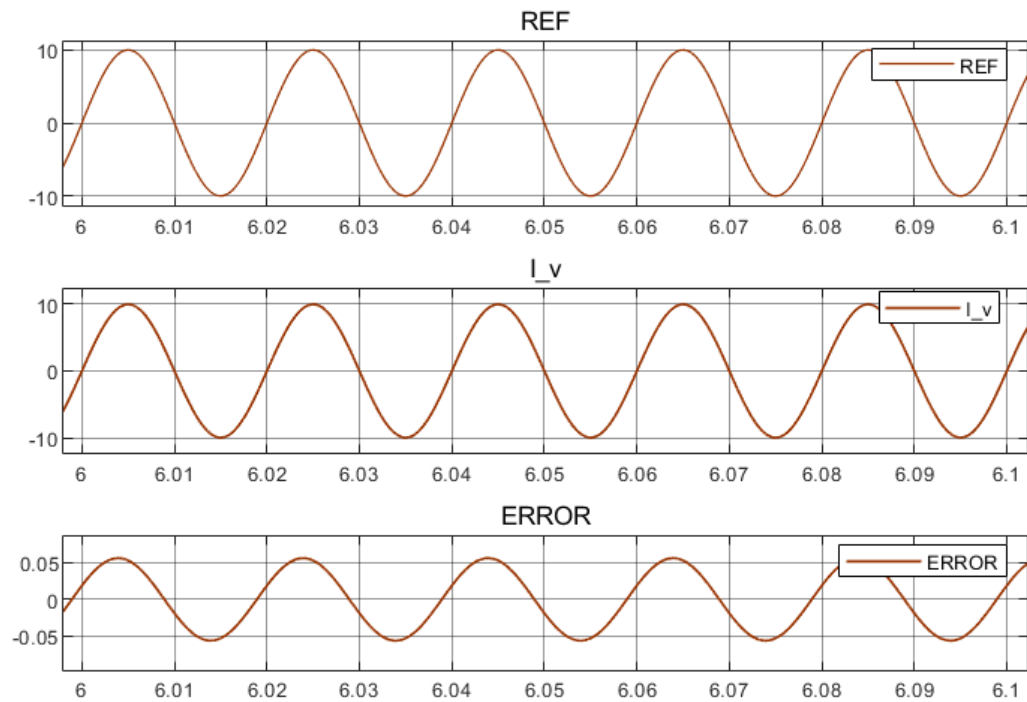


Figure 3.16 Output current reference, real and error graphs

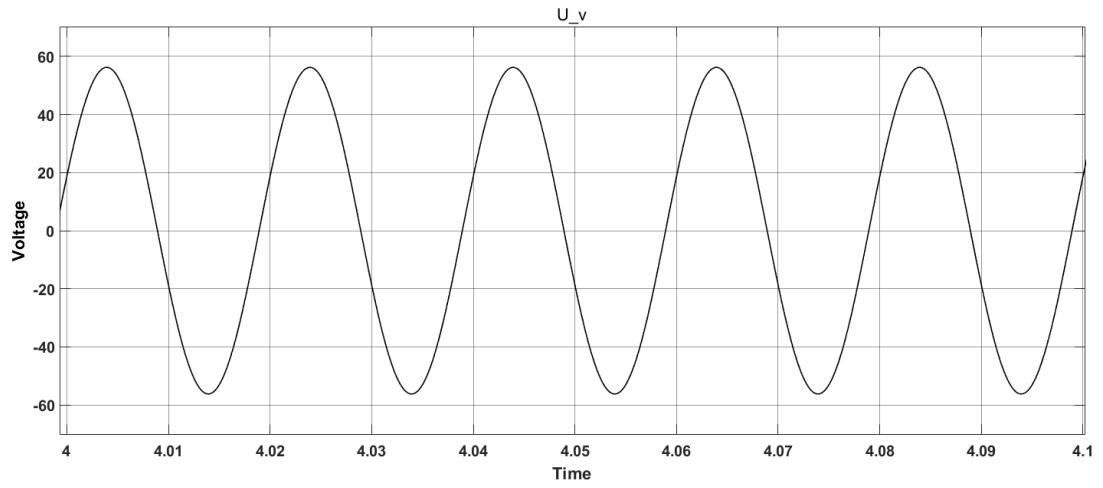
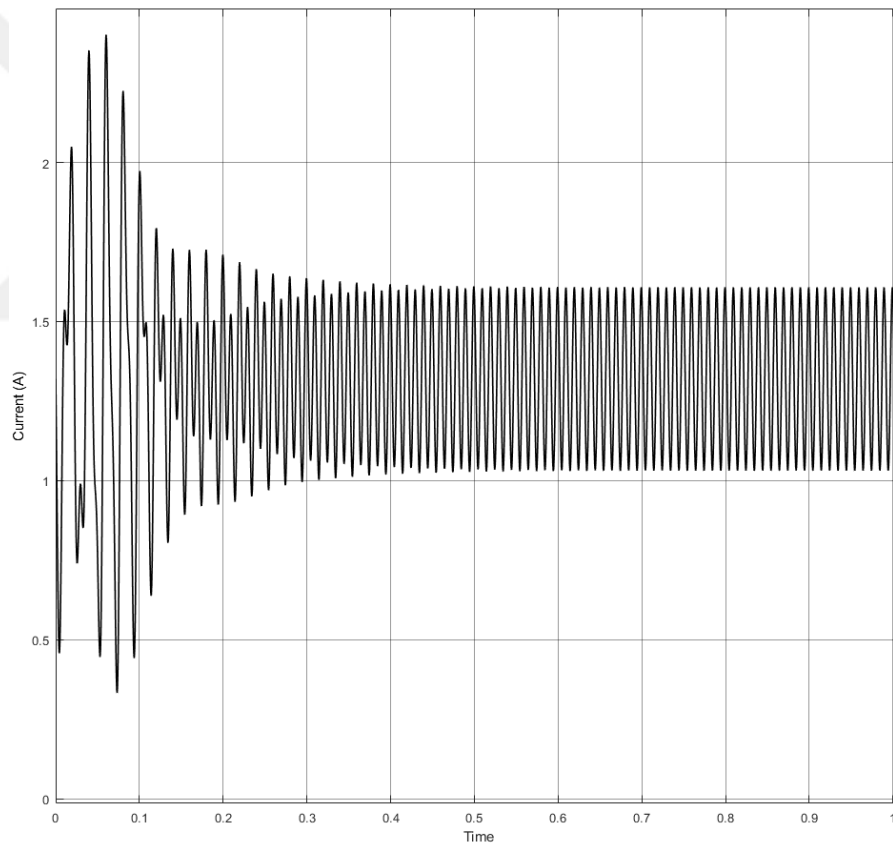
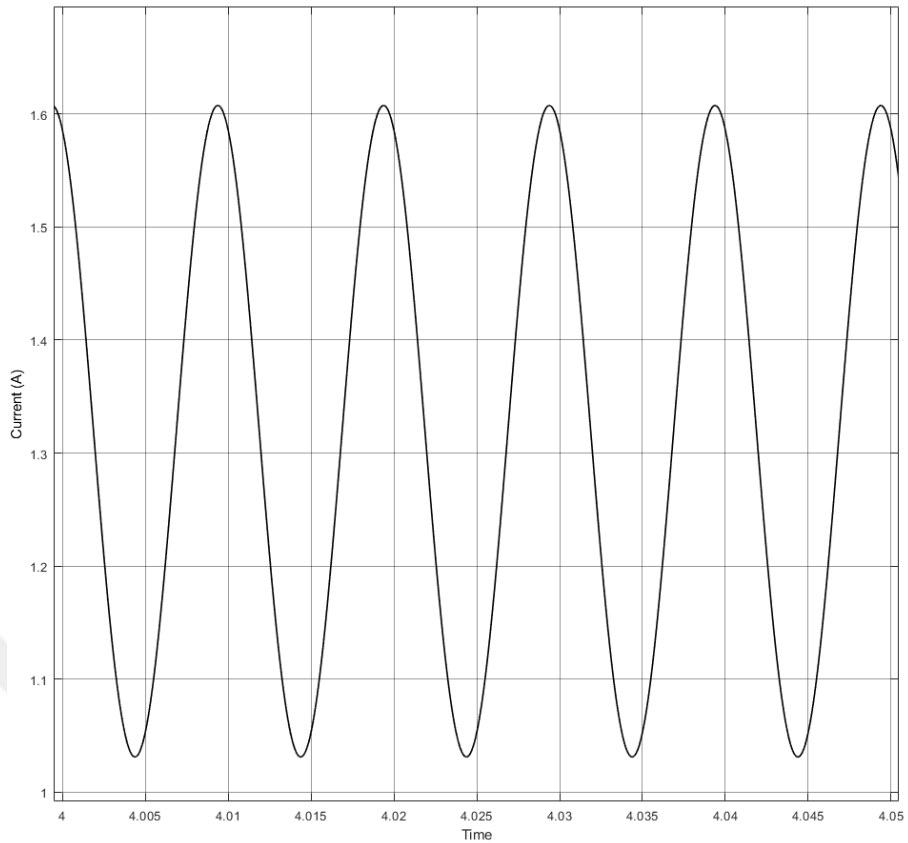


Figure 3.17 Generated Output Voltage



(a)

Figure 3.18 Differential current (a) initial and (b) steady state



(b)

Figure 3.18 continues

The dc part of differential current is same as the DC link current responsible for the real power flow and the ac circulated current is subjected to be minimized. The initial starting transients are small and the energy variations in time are also tracking around the reference values as shown errors on the energy given figures 3.19 and 3.20.

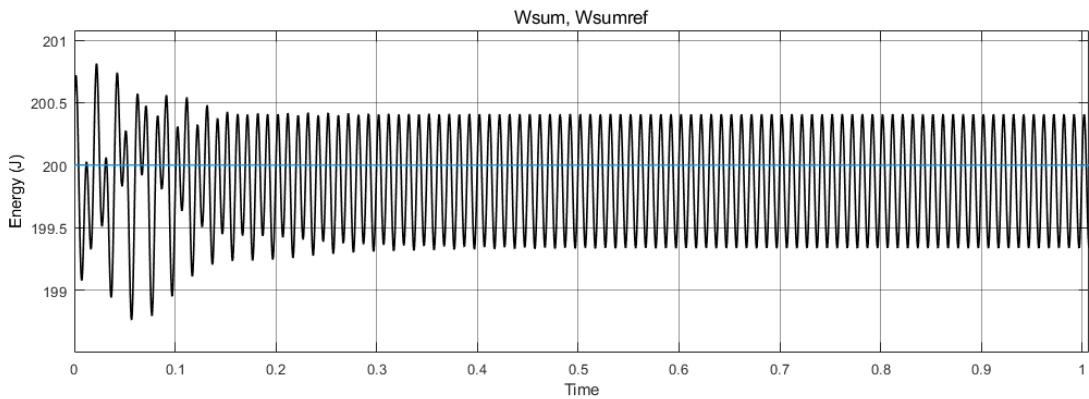


Figure 3.19 Total Energy of third model, (W^2)

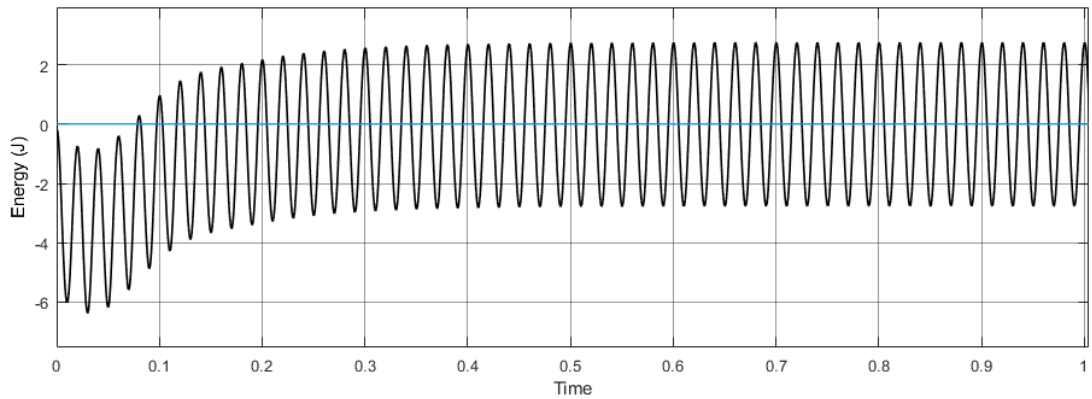


Figure 3.20 Difference of energy, (W^2)

3.4 Circulating Current Control with PR Controller

The circulating current is suppressed with the help of PR controller. The circulating current has the second harmonic (at the twice of grid frequency). The PR controller is tuned to 100 Hz. As seen from the figure 3.21 the differential current's dc part is subtracted by filtering by low pass filter and the rest of it is compared with the desired value which is zero. The error is passed through the PR controller.

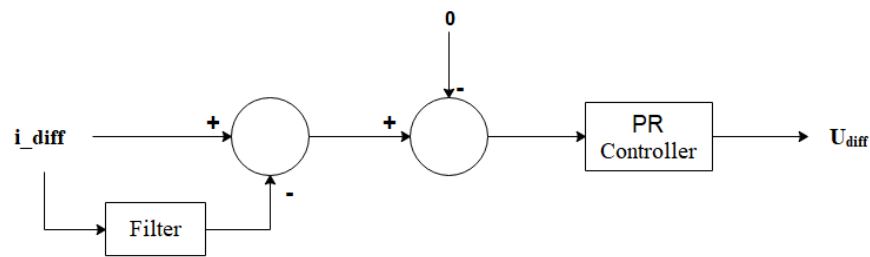


Figure 3.21 Differential current control part block diagram

The output of circulating current suppression method shown in figure 3.22 gives the reference value for the differential voltage needed to suppress the circulating current. This reference value is taken into the consideration according to equations (2.22) and (2.23) (Wang et al., 2017) and (Li et al., 2018).

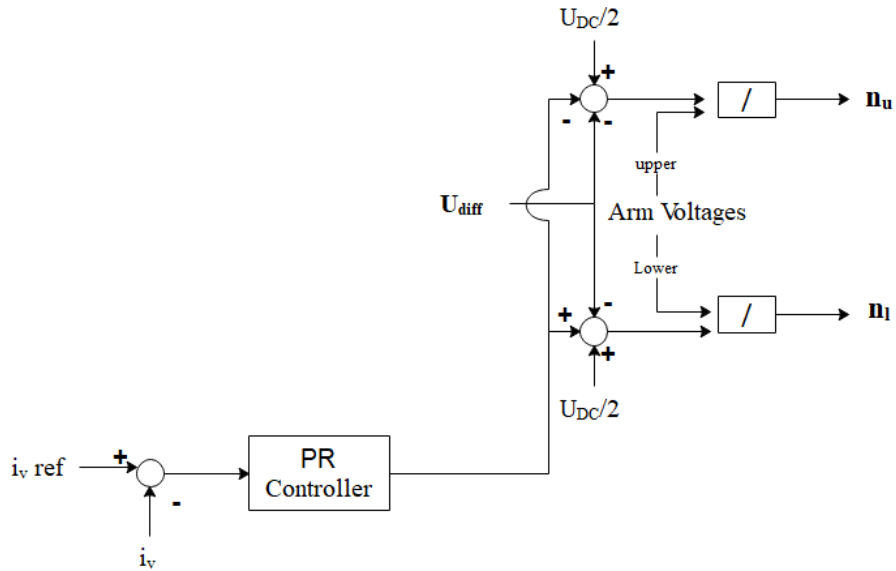


Figure 3.22 Differential current control algorithm common part

In this algorithm U_{diff} is generated from the circulating current error.

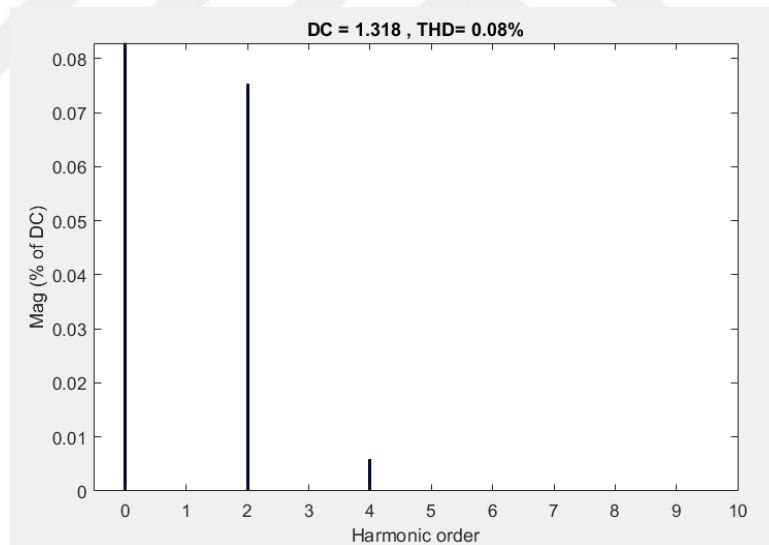


Figure 3.23 FFT Window of circulating current controlled model

Figure 3.23 shows the fast fourier transform (FFT) analysis of the differential current from the Simulink powergui toolbox. This method is more successful in reduction of circulating current. Only second and fourth order harmonics are appeared. However, their effects are very small with respect to the dc component. The total harmonic distortion rate is 0.08%.

3.4.1 Optimization of PR Parameters

MATLAB tools are used for the optimization of the parameters of PR controller. In this section usage of optimization tool and parameter selection will be discussed. First of all K_i and K_p parameters are defined as a variable in a workspace and their initial values are assigned. The second step goes through the response optimization. In this part there is an option for the sensitivity analysis. Sensitivity analysis is assigned for the desired step response parameters and the circulating current is selected in this work. The rest of the section describes the optimization process by using the MATLAB user toolboxes for indicating these steps. The transfer function given in figure 3.24 has the resonant frequency constant. Its value is 628 radian which is the two times of grid frequency.

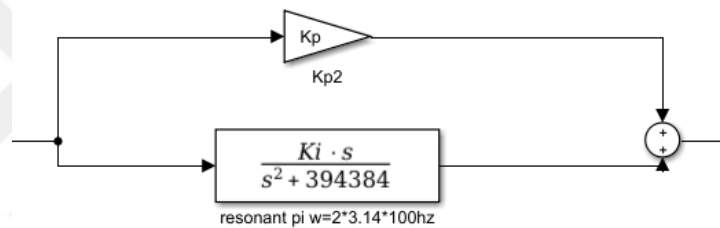


Figure 3.24 PR controller

The initial values given in figure 3.25 are assigned based on the experience of engineering point of view. If the initial values are closer values to optimized parameters, the simulation can terminate the solution faster.

The screenshot shows the MATLAB Workspace window. It contains a table with two columns: 'Name' and 'Value'. The first row shows 'Ki' with a value of 200. The second row shows 'Kp' with a value of 1.

Name	Value
Ki	200
Kp	1

Figure 3.25 Initial points of controller parameters

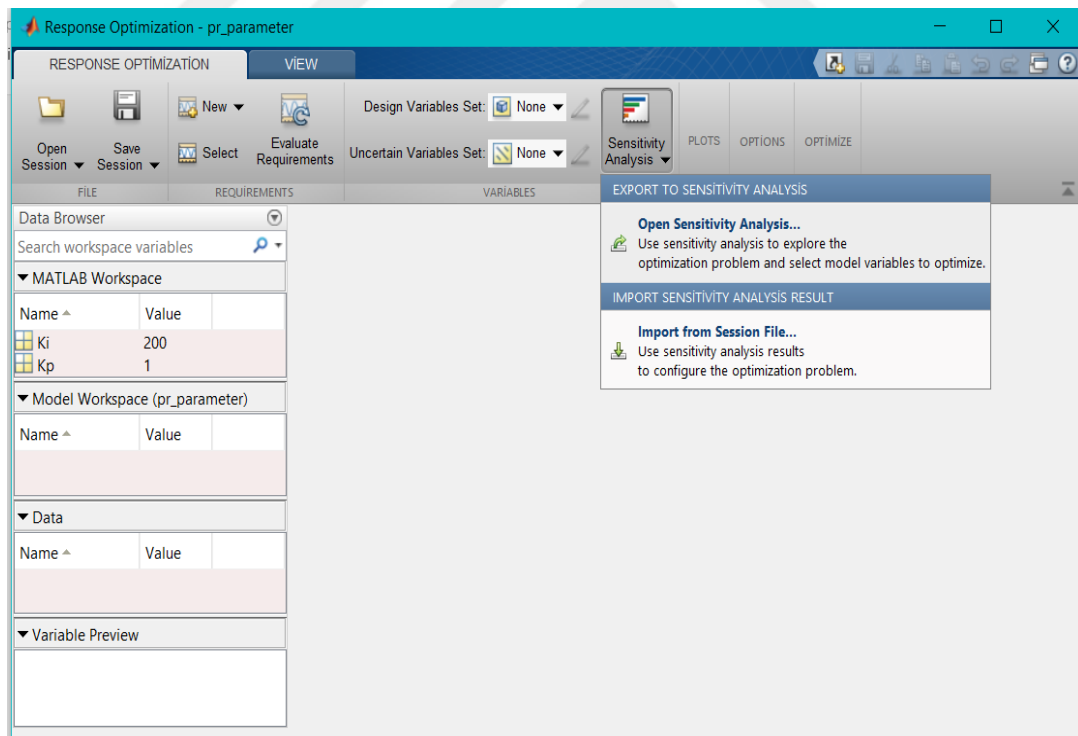
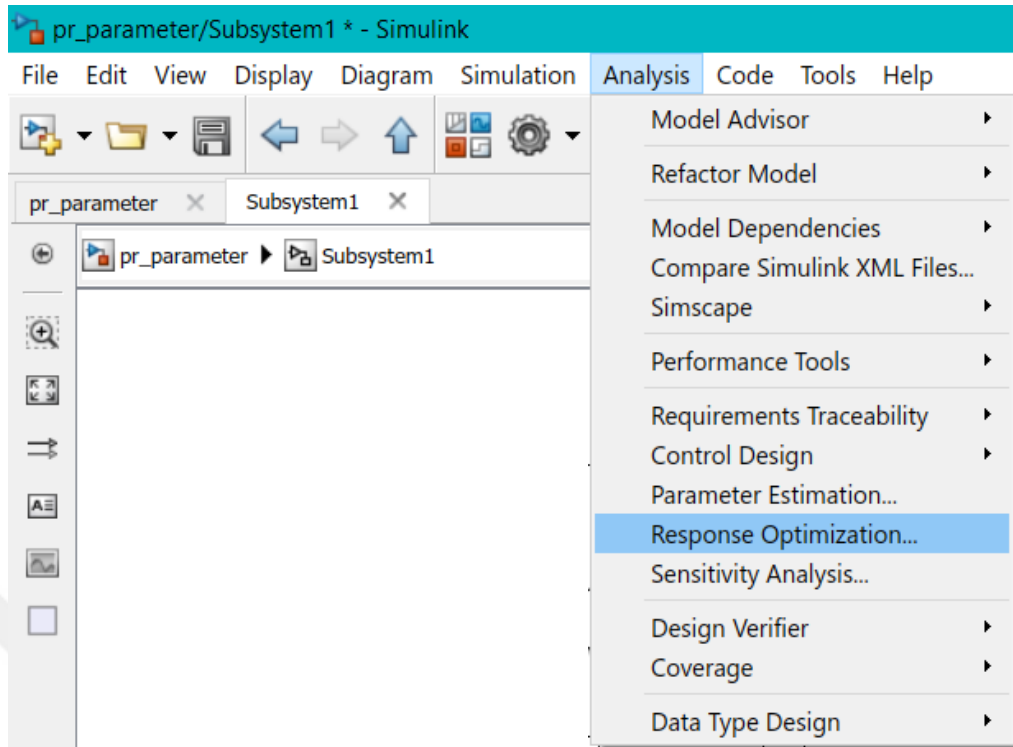


Figure 3.26 Flowchart for the use of optimization toolbox

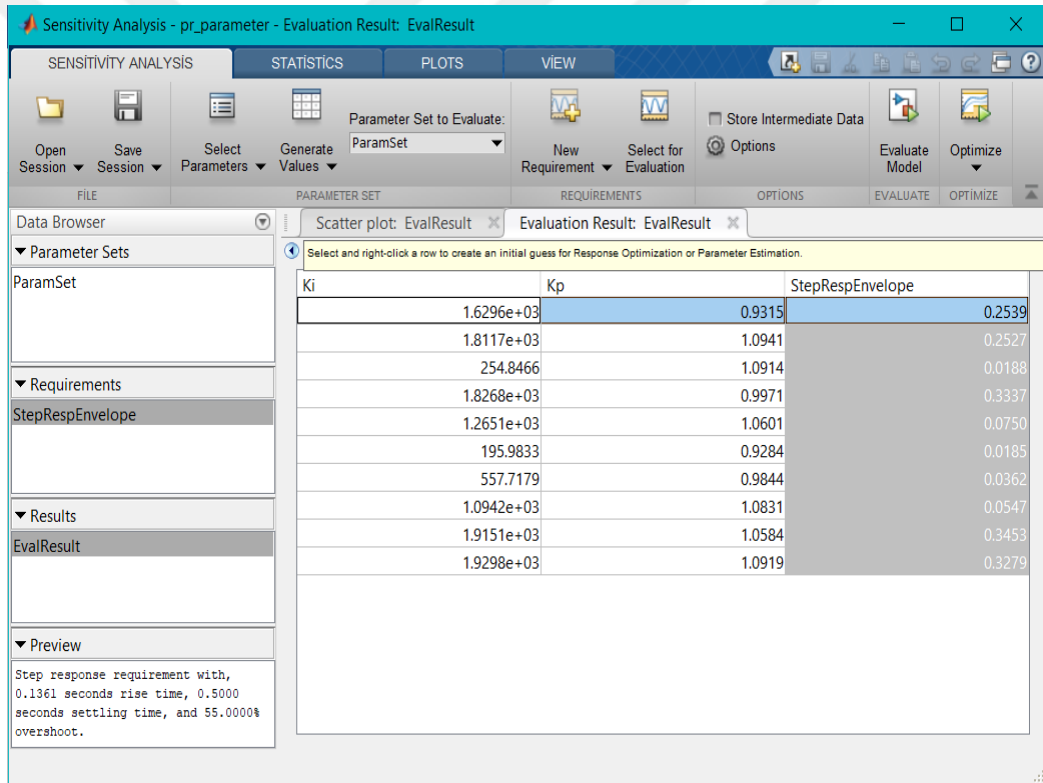
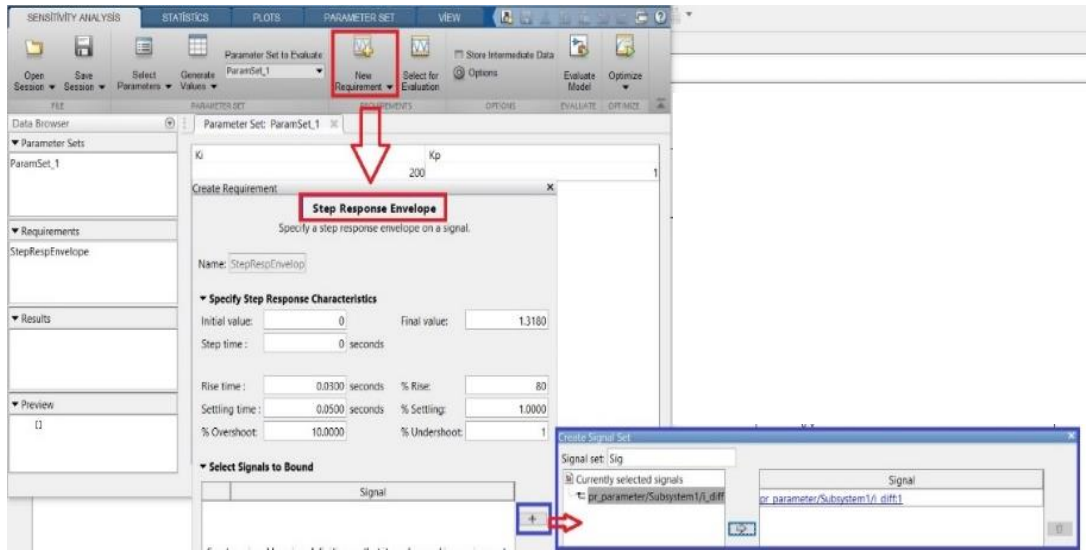


Figure 3.26 continues

In optimization part, after opening the sensitive analysis section the next step is choosing the desired signal which will be used as a parameter. Click on the desired line in Simulink file to select the signal. Then evaluate the optimization results according to the response of this signal.

The final step is selecting the right parameters of the lowest step response envelope. The bode graph given in figure 3.27 gives an opinion for selection.

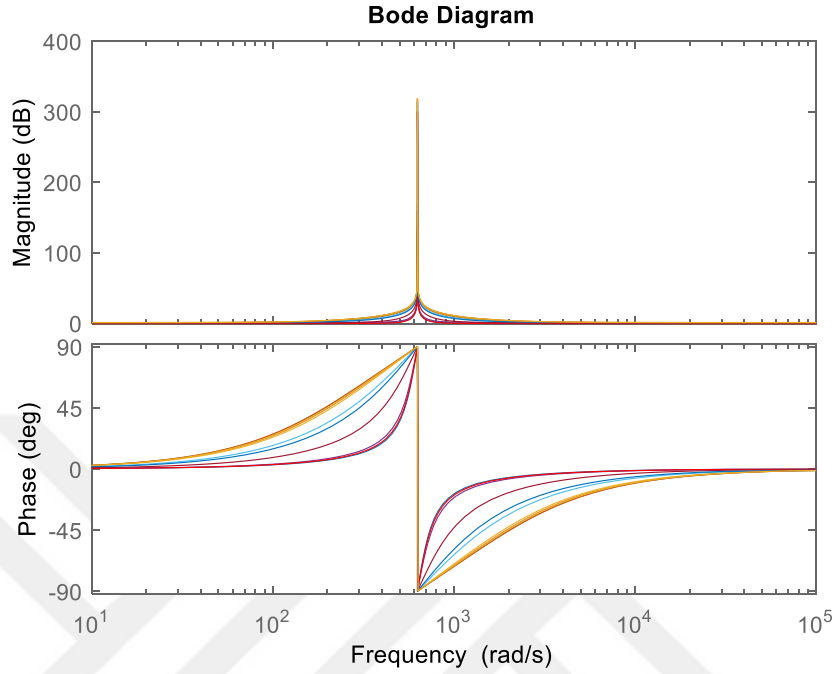


Figure 3.27 Bode diagram

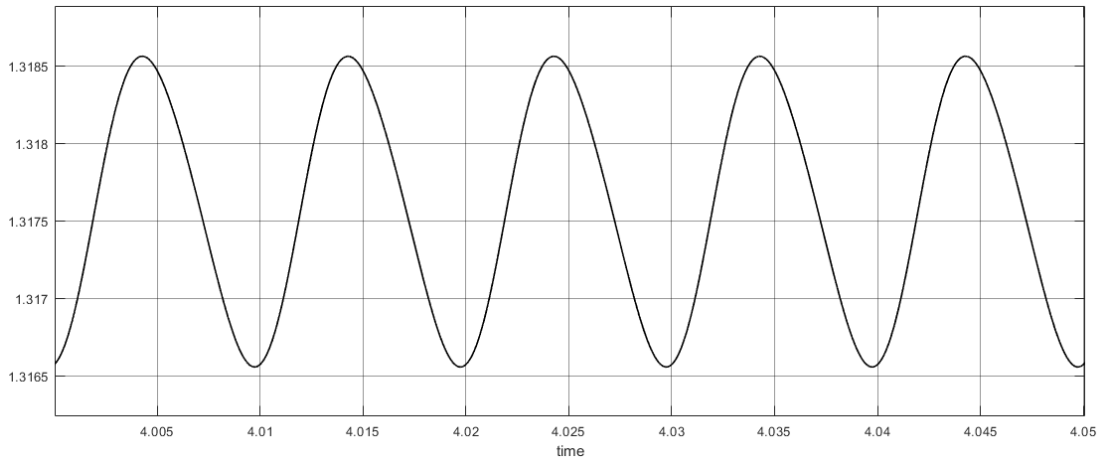
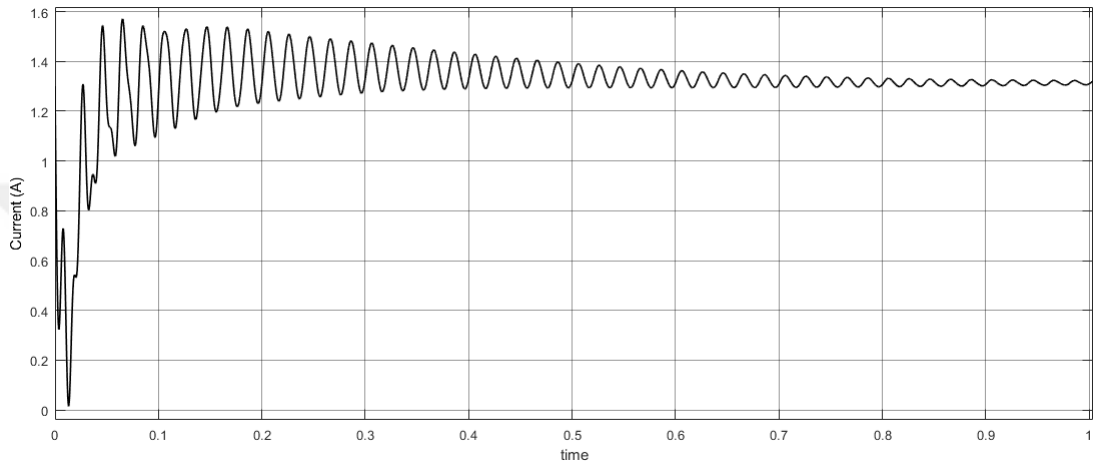
The bode diagram shown in figure 3.27, shows the best parameter combination for this system. The sequence and related K_i and K_p parameters are tabulated below.

K_i	K_p	
sys1	1.6296e+03	0.9315
sys2	1.8117e+03	1.0941
sys3	254.8466	1.0914
sys4	1.8268e+03	0.9971
sys5	1.2651e+03	1.0601
sys6	195.9833	0.9284
sys7	557.7179	0.9844
sys8	1.0942e+03	1.0831
sys9	1.9151e+03	1.0584
sys10	1.9298e+03	1.0919

Figure 3.28 Generated K_i and K_p parameter for optimization

3.4.2 Simulation Results

The results of simulation for the circulating current control are presented in this section. The results show that this controller is more successful to suppress the circulating current and the transients.



(b)

Figure 3.29 (a) Differential current and (b) its steady state

The peak to peak amplitude of the ac part is 0.002 and the dc component is 1.318 as shown in figure 3.28. The starting transients damp out in less then one second. The capacitor voltages shown in figure 3.29 is at the DC link voltage level with around 2 V peak to peak oscillation.

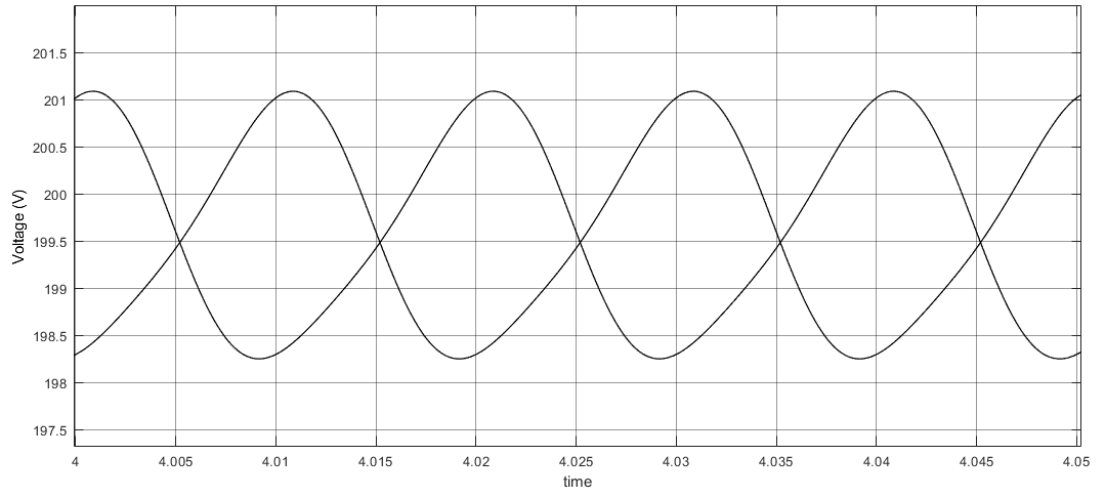


Figure 3.30 Capacitor voltages

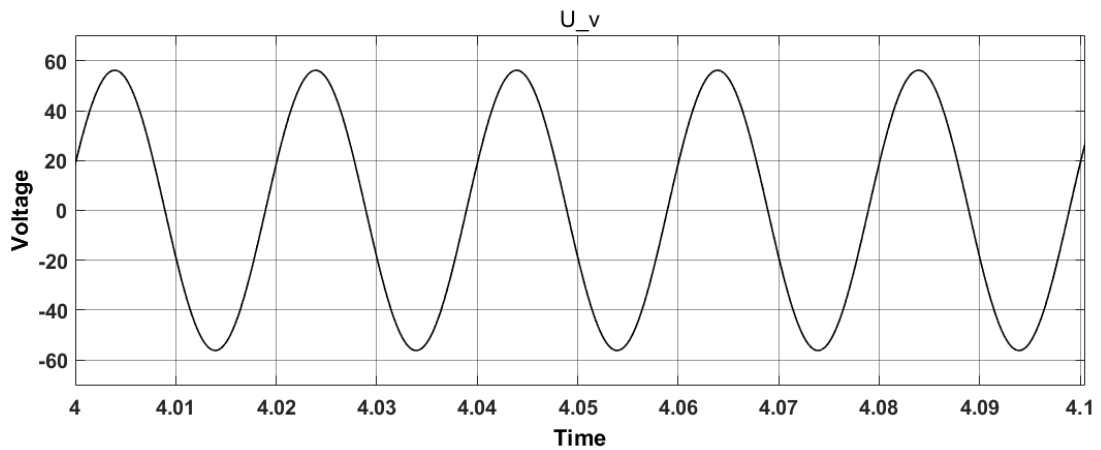


Figure 3.31 Generated output voltage of current controlled model

3.5 Comparison of Simulation Results of Four Different Analysis

In this section the results of the four different models are examined in per unit to compare the models responses. All of the results are generated by starting up the simulation with the same initial values in pu and solver.

The open loop model given in figure 3.32 has the biggest initial response and a circulating current component as expected. At starting almost half of the differential current is AC component and at steady state, this level is decreased up to 10 percent. It is not a huge response but it must be noted that there is an assumption about perfect voltage sharing between SMs.

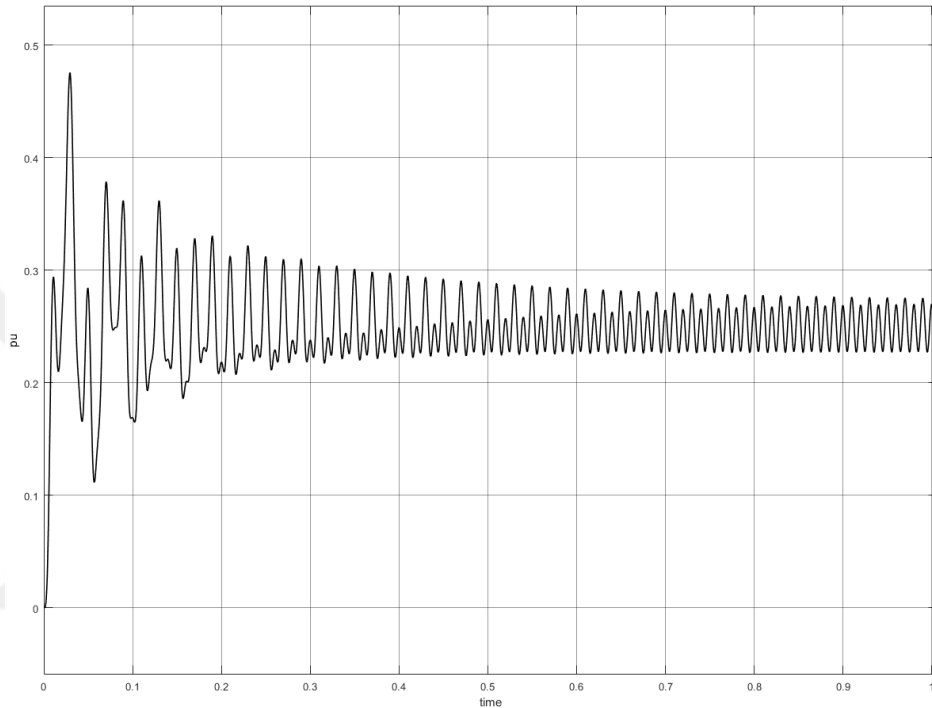


Figure 3.32 Differential current of open Loop model in per unit

With energy control algorithm, initial effect is suppressed at a level of twenty percent of output current. It is almost half of the previous one. Differently from the previous one, control algorithm forces the transients setting down. However, the AC magnitude still is high from the desired level. Figure 3.33 and 3.34 indicates the model behavior with some differences. First of all, for both second and third model energy control method is applied, however second one still has assumptions and uses output values from the reference, on the other hand, the third model evaluates the real system results. Thus, while in 3.33 starting transients a little bit less than the 3.34, settling time is longer.

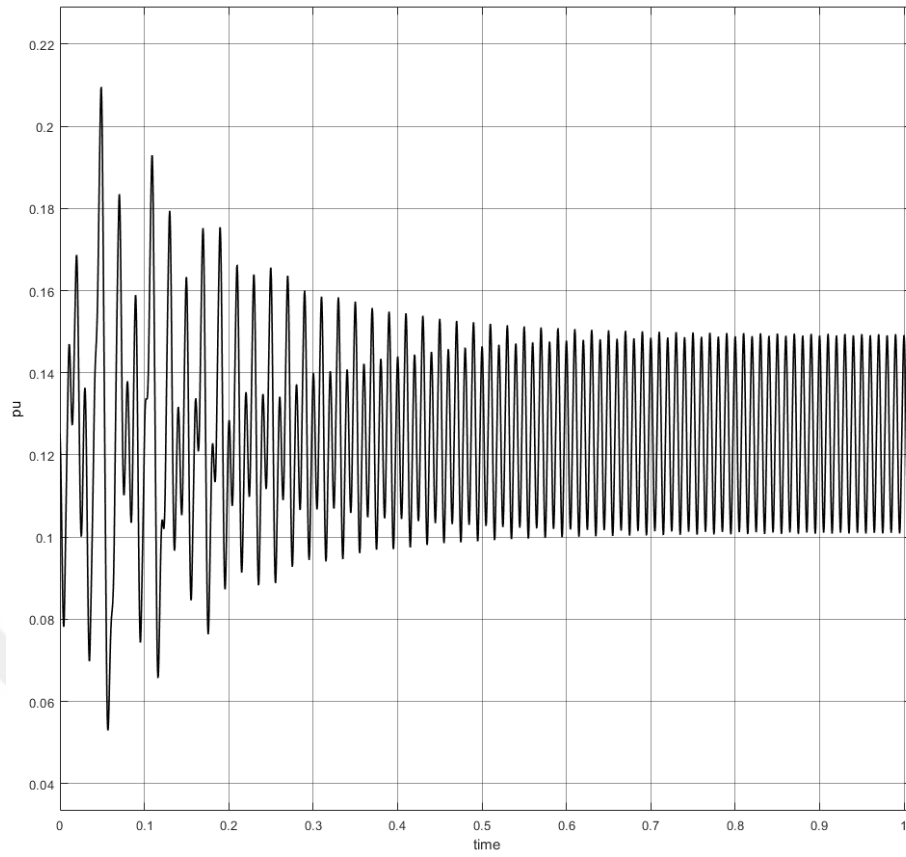


Figure 3.33 Differential current of second model in per unit

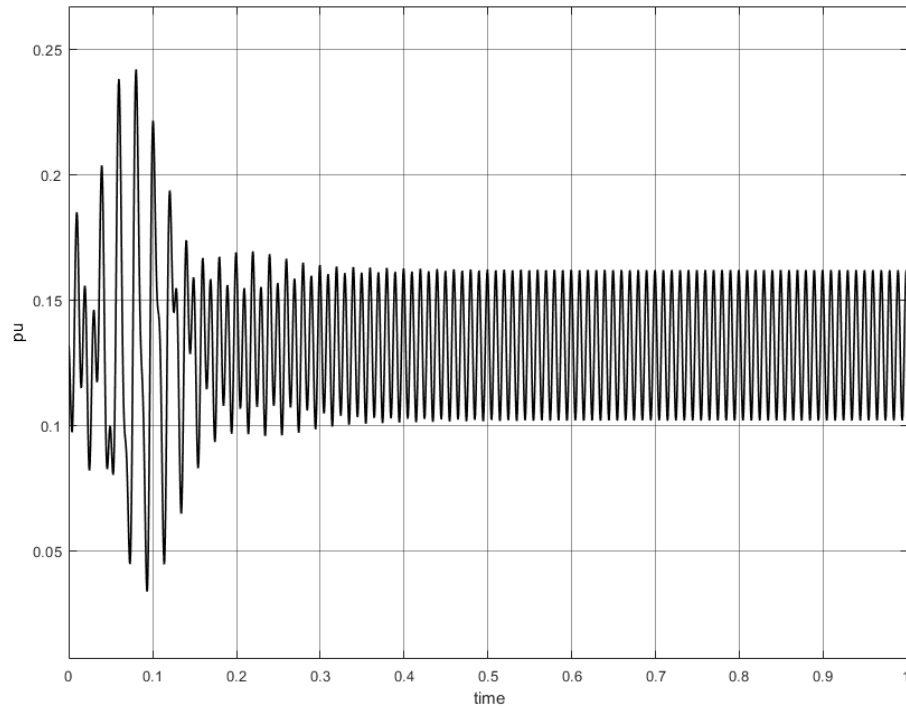


Figure 3.34 Differential current of third model in per unit

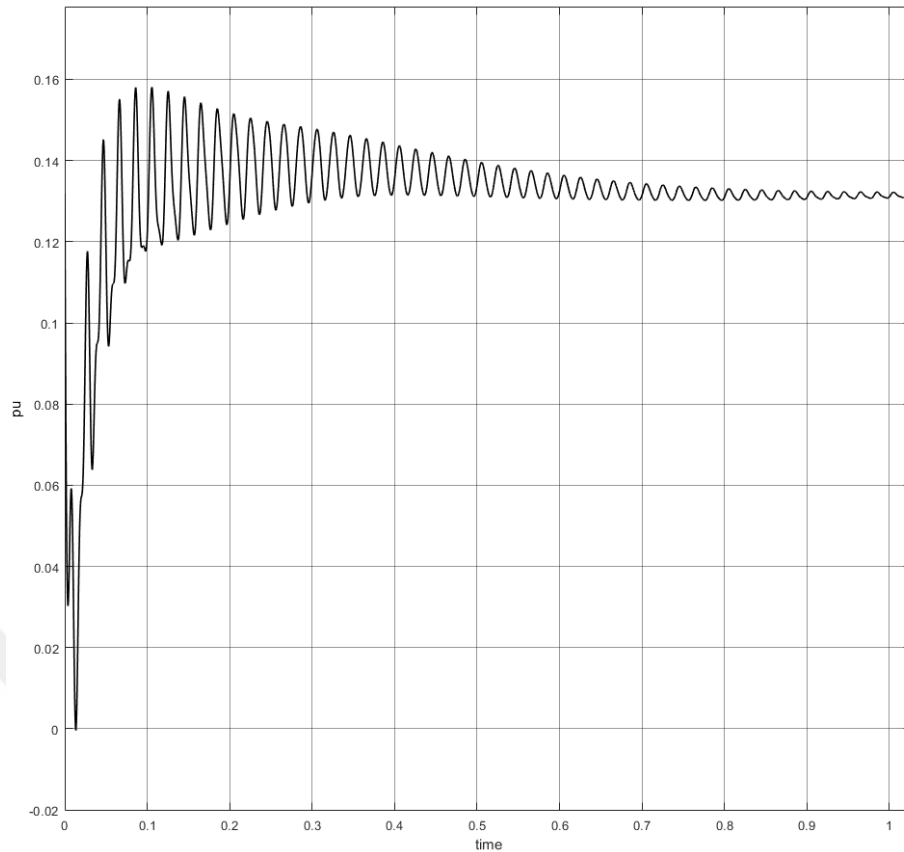


Figure 3.35 Differential current of current controlled model in per unit

The general behavior and rates of all models are as expected and unchanged in comparison with the real value model and per unit. Per unit result shows the algorithm effects on results more clearly in percentage.

In comparison, except from the open loop model, among controlled models; second and third models results are closed due the same logic the only difference is second model assumes some parts instead of controlling and it causes some neglection. Actually, results of the third model is the final version of this algorithm. Thus, it must be compared with differential current controlled model to understand the effect of these two algorithm.

As in previous result with real values, again in per unit results show up the last current controlled model is more successful in suppressing the circulating part than energy controlled model. The magnitude of ac part is decreased about 100 times and the initial overshoots almost cut in half.

3.6 Differential Current Analysis by Changing the Grid Frequency

The resonance frequency affects the magnitude of circulating current (Kalle et al., 2012). The highest resonant frequency is generated when modulation index (m) is equal to 1 and the second harmonic (n=2) is selected.

$$\omega_r = \sqrt{\frac{5}{48} \frac{1}{L_{arm} C_{arm}}} \quad (3.10)$$

According to the equation (3.10), the resonance frequency for the system is 13.27 Hz. To observe the effect of resonance condition on the circulating current, the average value model without the closed loop control (open loop model) is solved at the grid frequency changed from 5 Hz up to 70 Hz. The results of the simulation at these frequencies are given in figure 3.36 as the graphic.

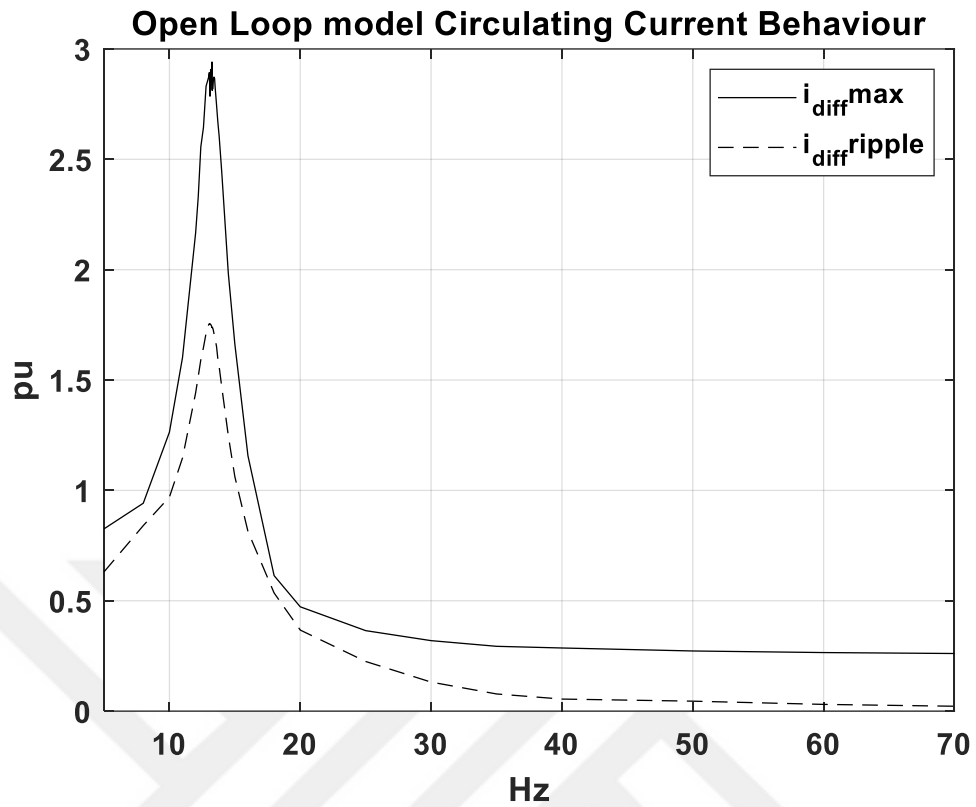
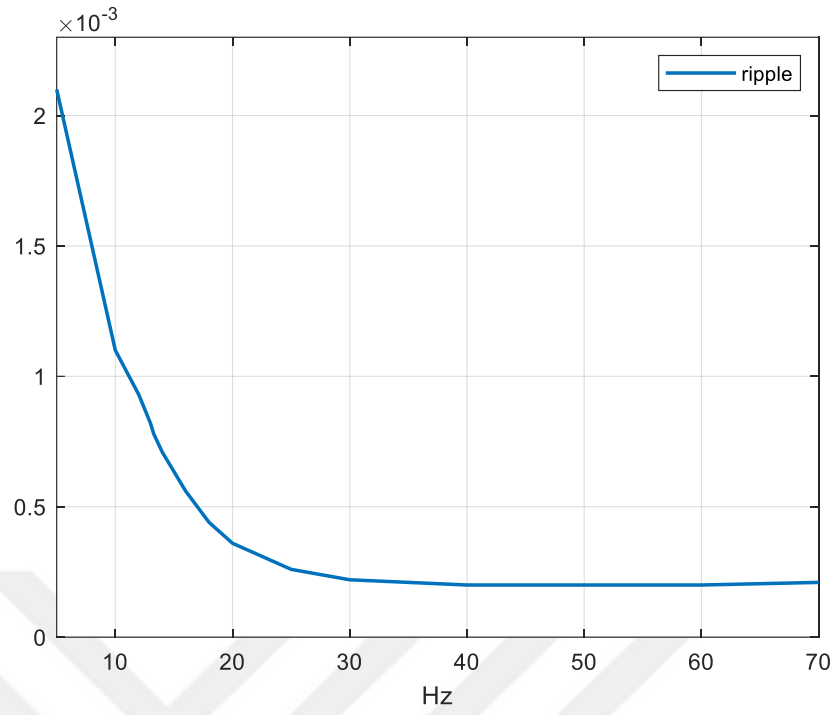
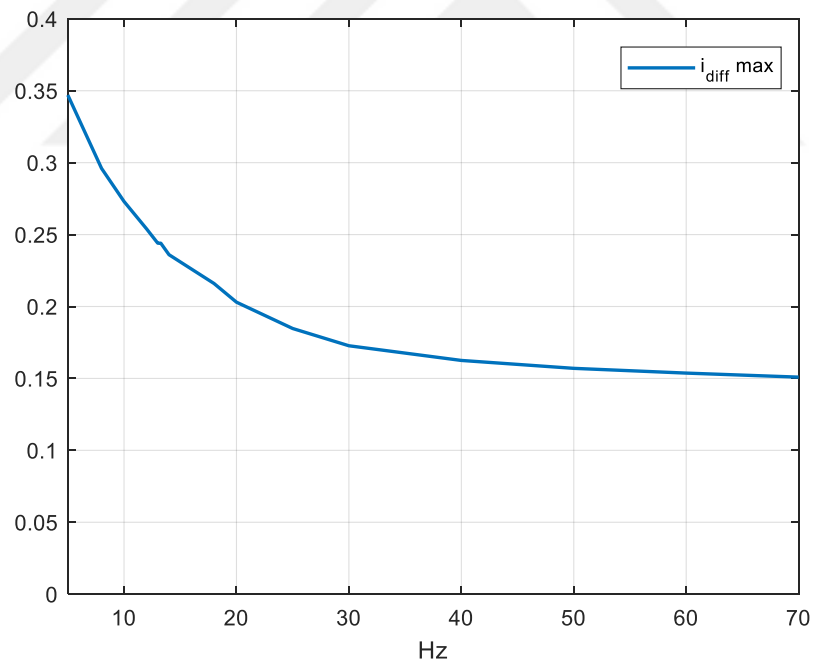


Figure 3.36 Change of differential current based on frequency in pu

The solid line indicates the peak to peak ripple magnitude of the circulating current and the dashed line is the peak amplitude of differential current in per unit. The system power loss is high around resonant frequency. Figure 3.37 shows the circulating current magnitude variation at different supply voltage frequencies (covering the resonance frequency) if the PR controller is enabled. The resonance is suppressed since the second harmonic is eliminated with the help of controller. PR controller is adjusted by the variable grid frequency.



(a)



(b)

Figure 3.37 Differential current behaviour in current controlled model depending on frequency (a) ripple (b) peak amplitude in per unit

CHAPTER FOUR

CONCLUSION

In this thesis, the energy control method based on the proportional differential controller and the average value model of the MMC are used together with the circulating current control. The control of the circulating current is carried out by using the proportional resonant controller and the entire system is analyzed in MATLAB/Simulink.

Firstly the state space form of the model (open loop model) is derived and analyzed to understand the main characteristics of the system, and observe the response of the system in ideal equalized submodule capacitor voltages. The existence of the circulating current in the system requires the suppression of it in order to reduce the converter losses and avoid the resonance. Control methods are implemented both based on energy and current control.

The controllers within the system model are compared in per unit and the most effective method that the circulating current is suppressed, is selected and examined for the resonance condition. The results show that the controller is significantly effective for suppressing the circulating current. This model is good enough to make decision on the effect of the resonance frequency depending on the harmonic components of circulating current and the modulation index. The results indicate that the resonance directly affects the magnitude of circulating current. The suppression of harmonic current components of the circulating current avoids the resonance in the system.

REFERENCES

- Antonopoulos A., & Angquist L., & Nee H. (2009). On dynamics and voltage control of the modular multilevel converter, *Power Electronics And Applications, EPE'09. 13th European Conference*, 1-10.
- Ängquist L., & Antonopoulos A., & Siemaszko D., & Ilves K., & Vasiladiotis M., & Nee H. P. (2010). Inner control of modular multilevel converters - an approach using open-loop estimation of stored energy, *The 2010 International Power Electronics Conference*, 1579 – 1585
- Ängquist L., & Antonopoulos A., & Siemaszko D., & Ilves K., & Vasiladiotis M., & Nee H. P. (2011). Open-loop control of modular multilevel converters using estimation of stored energy, *IEEE Transactions On Industry Applications*, 47 (6), 2516 - 2524
- Asimakopoulos P. (2013). *Design and control of modular multilevel converter in an active front end application*. Master Thesis, CERN, The European Organization for Nuclear Research, Göteborg, Sweden
- Beyhan E., & Akpinar E. (2019). Analysis and control of single phase grid connected modular multilevel converter in per unit, *4 International Mediterranean Science And Engineering Congress*, 109-112
- Glinka M., & Marquardt R. (2003). A new single phase ac/ac multilevel converter for traction vehicles operating on AC line voltage. *Power Tech Conference Proceedings IEEE*, Bologna, 3, 7 -12
- Glinka M., & Marquardt R. (2005). A new single phase ac/ac multilevel converter family, *IEEE Transactions On Industrial Electronics*, 52 (3), 662 - 669

- Hagiwara M., & Maeda R., & Akagi H. (2011). Control and analysis of the modular multilevel cascade converter based on double-star chopper- cells (MMCC-DSCC), *Power Electronics IEEE Transactions*, 26, 1649 -1658
- Hammond P. W. (1997). A new approach to enhance power quality for medium voltage AC drives. *IEEE Transactions On Industry Applications*, 33 (1), 202 - 208
- Harnefors L., & Antonopoulos A., & Norrga S., & Angquist L., & Nee H. P. (2013), Dynamic analysis of modular multilevel converters, *IEEE Transactions On Industry Applications*, 60 (7), 2526–2537
- Ilves K., & Antonopoulos A., & Norrga S., & Nee HP. (2012). Steady state analysis of interaction between harmonic components of arm and line quantities of modular multilevel converters. *IEEE Transactions On Power Electronics*, 27 (1), 57 - 68
- Ilves K., & Antonopoulos A., & Norrga S., & Harnefors L., & Nee HP. (2014). On energy storage requirements in modular multilevel converters. *IEEE Transactions On Power Electronics*, 29 (1), 77 - 87
- Jinke L., & Konstantinou G., & Wickramasinghe R. H., & Pou J., & Wu X., & Jin X. (2018). Impact of circulating current control in capacitor voltage ripples of modular multilevel converters under grid imbalances. *IEEE Transaction On Power Delivery*, 33, 1257 - 1267
- Lescinar A., & Marquardt R. (2003). An innovative modular multilevel converter topology suitable for a wide power range. *IEEE Bologna Power Tech Conference Proceedings*, Bologna, Italy; 3 (6)
- Lescinar A., & Marquardt R. (2003). A new modular voltage source inverter topology. *In proceedings of the European Power electronics conference (EPE)*, Toulouse, France; 1- 10

- Marquardt R., & Lescinar A. (2004). New concept for high voltage – modular multilevel converter. *IEEE PESC*, Aachen, Germany.
- Meynard T. A., & Foch H. (1992). Multilevel conversion: high voltage choppers and voltage source inverters. *IEEE Power Electronics Specialists Conference*, 397-403
- Nabae A., & Takahashi I., & Akagi H. (1981). A New Neutral Point Clamped PWM Inverter, *IEEE Transactions on Industry Applications*. IA-17 (5), 518-523
- Teoderescu R., & Blaabjerg F., & Liserre M., & Loh P. C., (2006). Proportional-resonant controllers and filters for grid-connected voltage-source converters. *IEEE proceedings electric power applications*. 153 (5), 750-762.
- Teoderescu R., & Liserre M., & Rodriguez P. (2011). *Grid converters for photovoltaic and wind power systems*. Chichester West Sussex : Wiley.
- Teodorescu R., & Zarri L. (2012). *Modular multi-level converter: modeling, simulation and control in steady state and dynamic conditions*. Department of Energy Technology, Aalborg University Denmark. Retrieved November 6, 2017, from <https://projekter.aau.dk/projekter/files/63645060/THESISrevFinale.pdf>
- Wang J., & Liang J., & Wang C., & Dong X. (2017). Circulating current suppression for MMC-HVDC under unbalanced grid conditions, *IEEE Industry Applications*, 53, 3250 – 3258

APPENDICES

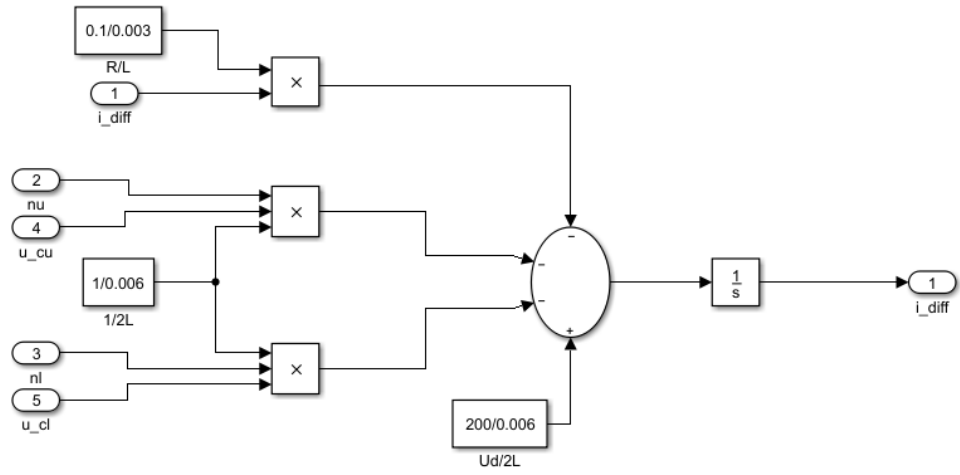


Figure A.1 Inside of the first MATLAB block, calculation of the differential current

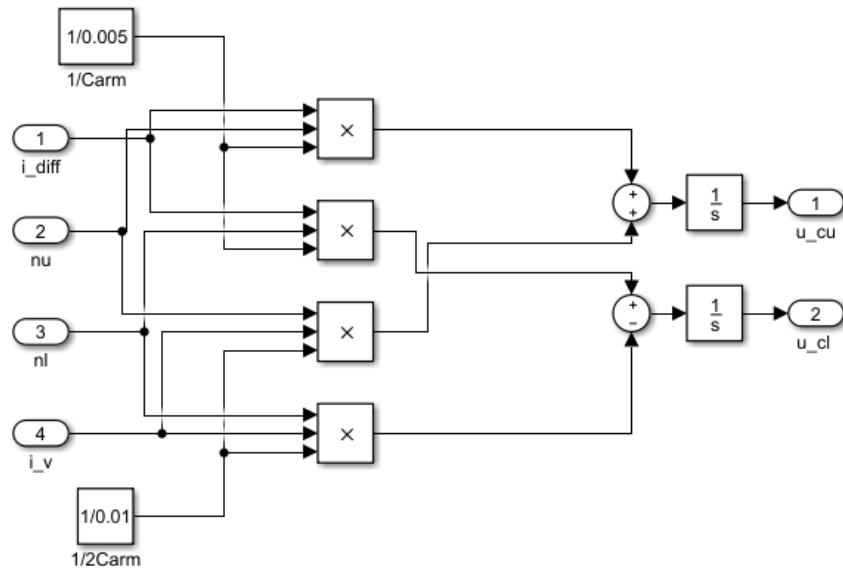


Figure A.2 Inside of the third MATLAB block, calculation of the arm voltages

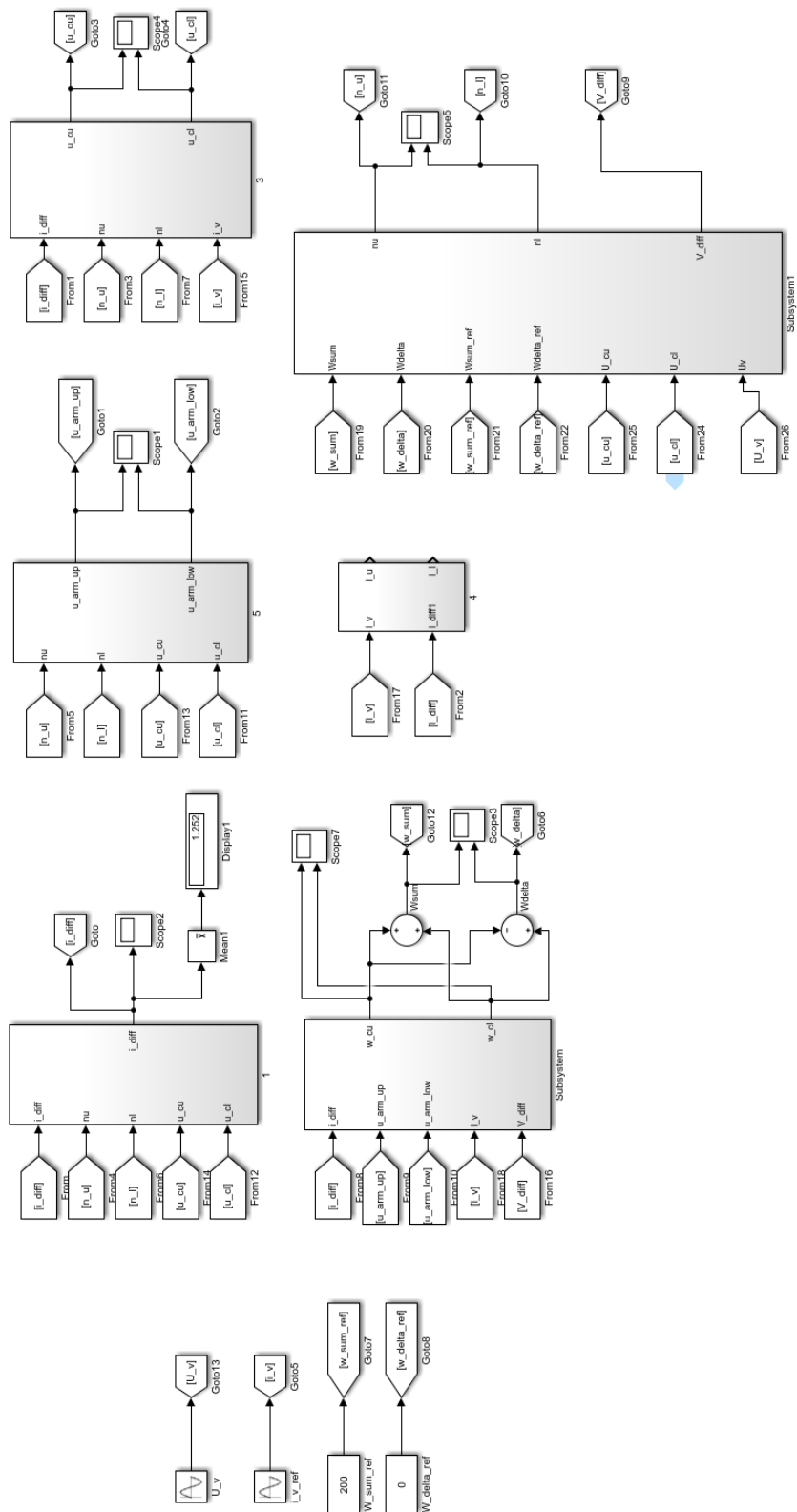


Figure A.3 Second energy controlled model MATLAB blocks

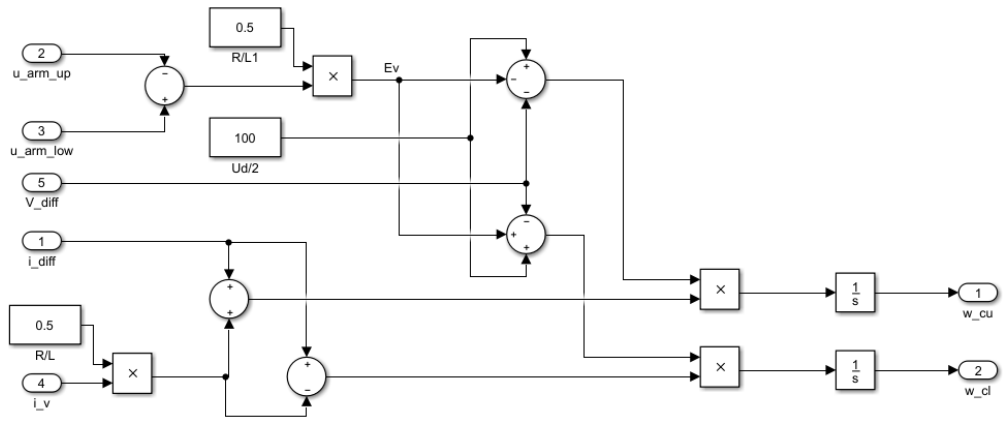


Figure A.4 Inside of the energy calculation MATLAB block

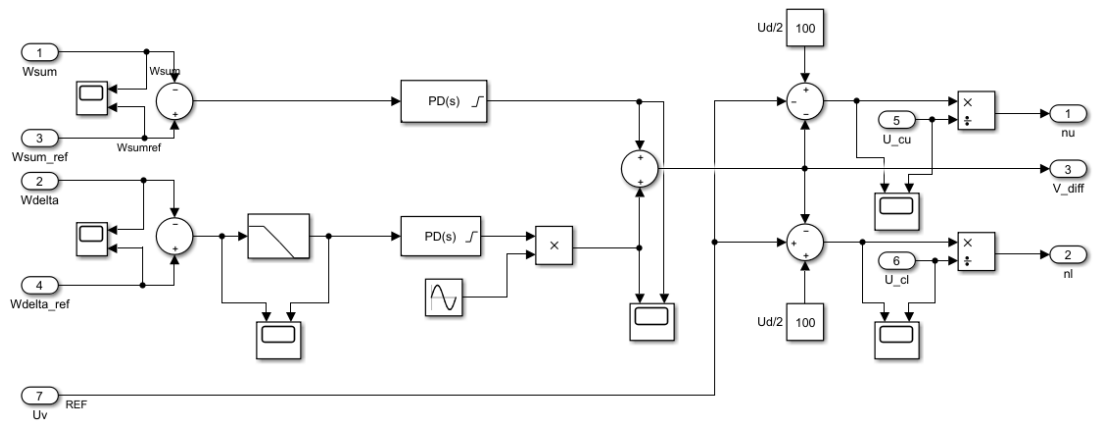


Figure A.5 Second model control block

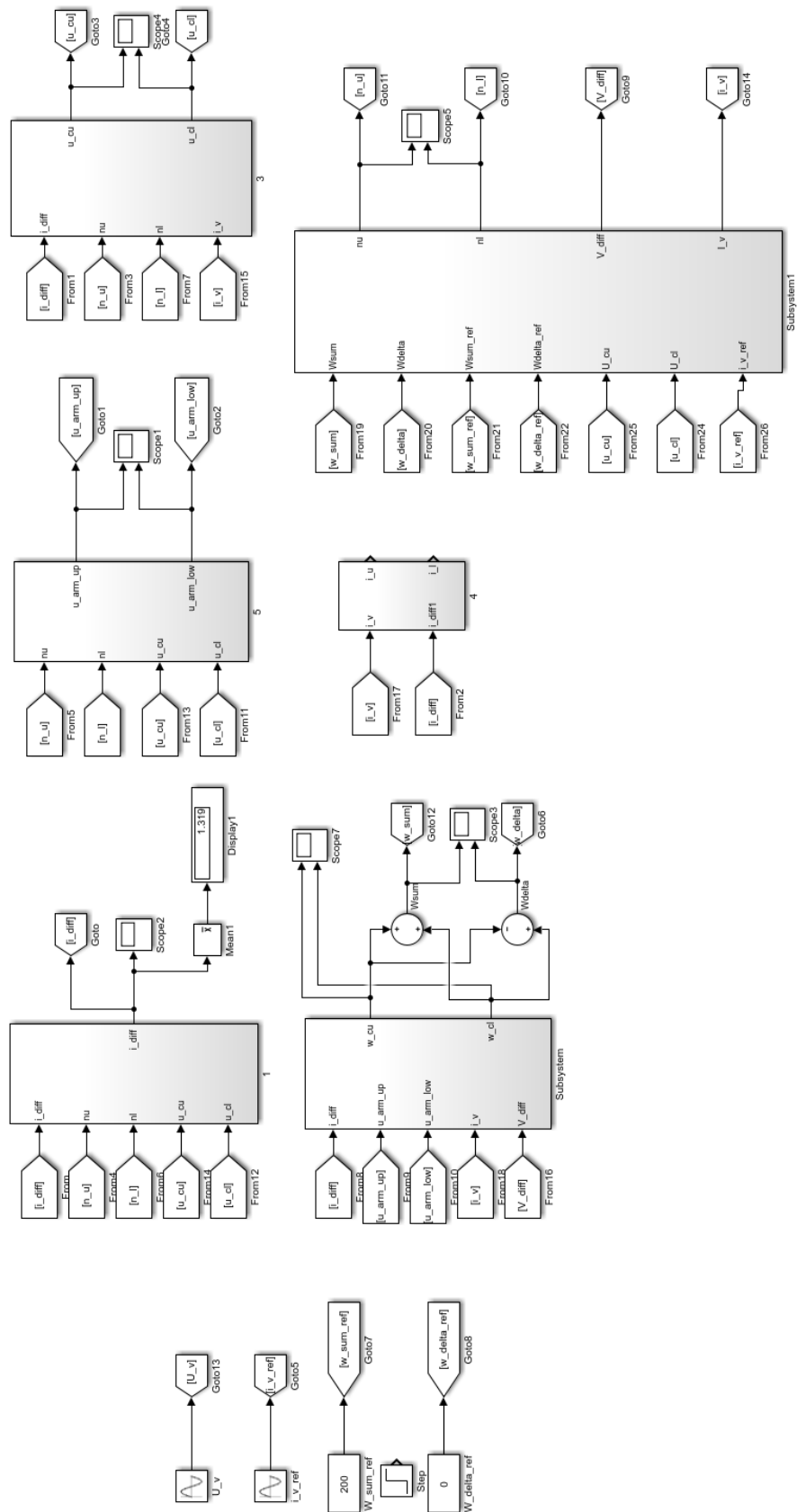


Figure A.6 Third model MATLAB blocks

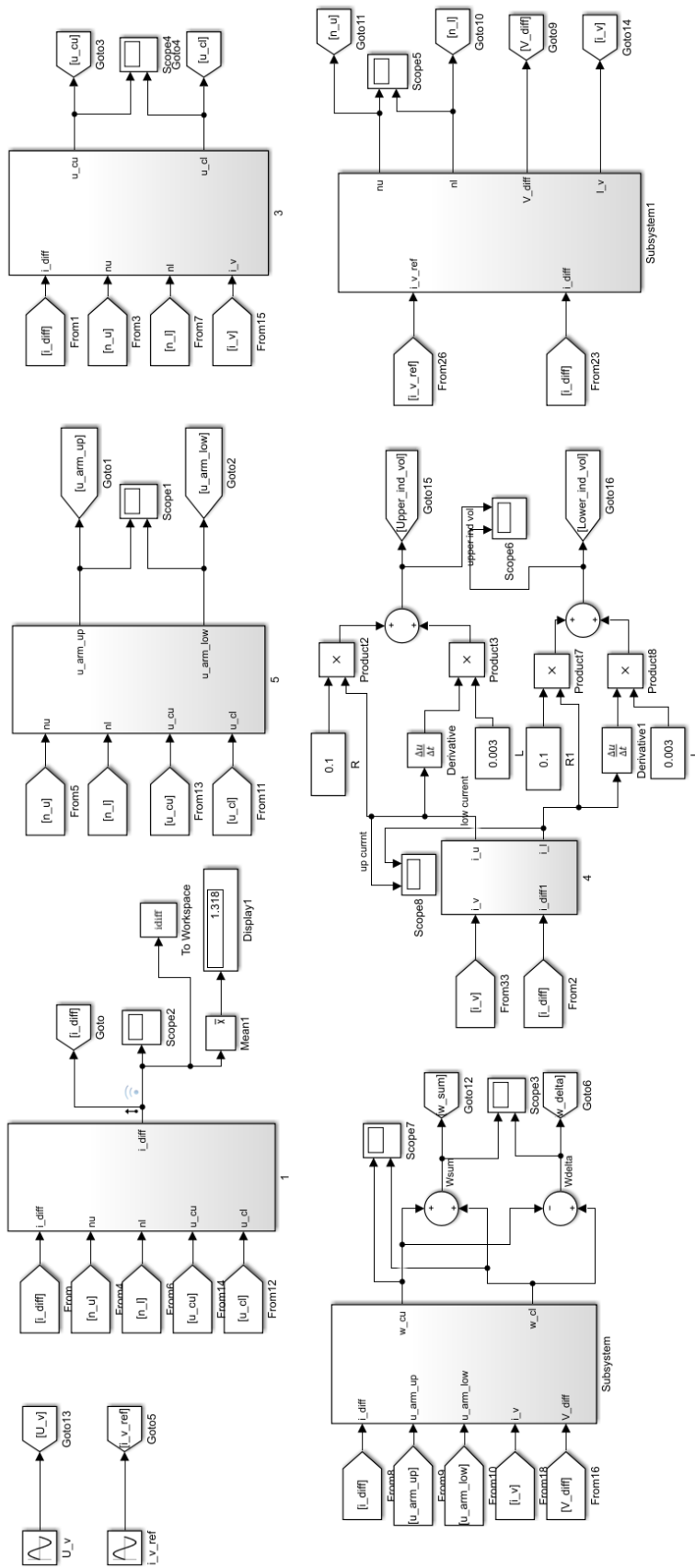


Figure A.8 Circulating current controlled model MATLAB blocks